Time scales and optical dephasing measurements: Investigation of dynamics in complex systems

Y. S. Bai and M. D. Fayer
Department of Chemistry, Stanford University, Stanford, California 94305
(Received 17 October 1988)

A detailed theoretical analysis of optical dephasing measurements performed on complex systems, e.g., glasses, proteins, or complex crystals, is presented. Unlike simple crystals, such systems undergo dynamical processes which have a very broad rate distribution. Dynamics can occur on a variety of time scales ranging from subpicoseconds to seconds, or longer. The formalism is based on a four-point correlation-function description of line-narrowing experiments. The results of optical dephasing measurements (time domain) or linewidth measurements (frequency domain) depend on a time T_W which defines the time scale associated with the particular experimental technique. Detailed information about the rate distribution of the system's dynamics is obtained from the change in the optical dephasing rate as the experimental time scale is changed, not from the dephasing rate measured in any individual experiment. A fundamental result, which is independent of the nature of the rate distribution or the coupling to the optical center, is proven; i.e., the derivative of the optical dephasing rate with respect to T_W, the experimental time scale, is directly proportional to the Laplace transform of the fluctuation rate distribution. As examples, the formal results are applied to two types of systems, optical centers in a glass and in a complex crystal. For the crystalline system Pr^{3+}:CaF_2, T_W-dependent optical dephasing data from the literature are analyzed quantitatively, where previously only a qualitative description was possible.

I. INTRODUCTION

In this paper we will develop a basic and general spectroscopic approach to the investigation of materials with complex dynamics. In systems other than simple crystals, e.g., a glass, dynamical processes can occur on times scales that range from subpicosecond to literally hundreds of years. In a simple crystal, dynamics involves fast-phonon-induced fluctuations about an equilibrium structure. In an amorphous material, in addition to fast-phonon fluctuations about a local structural configuration, evolution of the local structure can take place over a vast range of time scales. In a complex crystal, nonphonon degrees of freedom, such as the local magnetic spin state, can undergo fluctuations at much slower rates than the phonon fluctuations. Macromolecules, such as proteins, have an extensive number of structural conformations separated by a wide variety of potential barriers. Conformational dynamics occur on many time scales. While it is well known that the dynamics of the local environment influence the dephasing process of the optical centers embedded in complex materials, a detailed connection between dephasing measurements in these systems and system dynamics has been lacking.

The dephasing of optical centers is induced by time-dependent perturbations of the energy levels involved in the optical transition. In simple crystals, the dephasing is induced by phonons, and the emphasis has been on understanding the nature of the intermolecular interactions that couple the optical center to the phonon bath. This is because the distribution of fluctuation rates associated with the phonon bath is known. For example, McCumber and Sturge studied the temperature-dependent optical dephasing of Cr^{3+} in ruby.[1] Their theoretical analysis and the more recent infinite-order theoretical treatment of the data by Skinner and Hsu[2] focused on the strength of the coupling to the acoustic phonons. The fluctuation-rate distribution was included in the calculation through the Debye density of states that describes the acoustic phonons. This study and others (see, e.g., references in Ref. 2) have produced extensive information on the interactions between optical centers and phonons.

In complex systems, the problem is fundamentally different. In addition to phonon-induced dephasing, optical dephasing can be caused by fluctuations of localized perturbers, such as the electric and magnetic moments of the host matrices. The fluctuation-rate distribution of these perturbers is unknown. The problem is to extract information on the dynamics occurring in the medium through the influence of dynamics on the dephasing of the embedded optical centers.

Experimentally, a variety of line-narrowing techniques have been used to measure optical dephasing. These include two-pulse photon echoes,[3] fluorescence line narrowing,[4] phosphorescence line narrowing, accumulated grating echoes,[5] incoherent echoes,[6] saturation optical hole burning,[7] and permanent optical hole burning.[8] In simple crystals, all of these experiments would be expected to measure the same optical dephasing rate, referred to as the homogeneous dephasing rate, $1/T_2$. It has been assumed by many that all of these techniques will measure the same optical dephasing rate in complex systems. Re-

cently, optical dephasing experiments on complex crystals[9] and experiments[10,11] and detailed theory[11,12] on glasses have proven that the various techniques, when applied to the same sample, do not measure the same optical dephasing rate.

The key is the differences in time scales associated with the various techniques. Complex systems have dynamics occurring on many time scales. Techniques operating on different times scales are sensitive to different aspects of the dynamics. Utilizing this fact quantitatively can unlock a door into the details of the distribution of rates of dynamical processes.

In a two-pulse photon-echo experiment, where the two pulses are separated by an temporal interval τ, the dephasing of the optical polarization is predominantly caused by the perturbers whose fluctuation rates are comparable to $1/\tau$. If the fluctuation of the perturbers is much faster than τ, the induced phase error in the optical polarization tends to be averaged out, resulting in "motional narrowing."[13] If, on the other hand, the fluctuation is much slower than τ, a significant portion of the perturbers remain static during the measurement. As a result, the induced transition frequency detuning of the optical center appears to be static inhomogeneous broadening and is rephased by the echo pulse sequence. Thus the characteristic time scale of the measurement is determined by the temporal separation between the two pulses, τ, which is usually on the order of the measured dephasing time itself. At low temperature (<5 K) this is typically picoseconds to nanoseconds for organic materials and nanoseconds to microseconds for inorganic materials.

In contrast, techniques such as stimulated echoes[14] and hole burning involve two time scales. Besides a short time scale τ, analogous to that in the two-pulse echo, there is a relatively long time scale, T_W. T_W is either the waiting time between the third pulse and the second pulse in a stimulated echo experiment or the waiting time between the reading pulse and the burning pulse in a hole-burning experiment. In the latter case, T_W is typically on the order of minutes, many orders of magnitude longer than τ. Like the two-pulse–echo case, the dephasing rates measured with these techniques arise predominantly from the contributions of the perturbers with fluctuation rates that fall into a certain range. The important difference is that now the range is given by $(1/T_W, 1/\tau)$, instead of being around $1/\tau$ as in the two-pulse–echo case. This makes these measurements, particularly hole burning, sensitive to slow fluctuations. If the fluctuation rates R of most perturbers fall in the range $1/T_W < R < 1/\tau$, the optical dephasing rates measured with hole burning, stimulated echoes, or other line-narrowing techniques can differ significantly from that measured with the two-pulse echo.

Thus the term "homogeneous linewidth," which is generally taken to be the dephasing rate measured in any line-narrowing experiment, is not well defined in complex systems. Because the two-pulse photon echo is the only optical line-narrowing experiment with $T_W=0$, it should measure the slowest dephasing rate. The dephasing rate measured by the two-pulse echo has been used as the operational definition of the homogeneous linewidth.[11]

Due to the variety of local environments associated with the perturbers, the fluctuation rates are often distributed over a broad range. This is particularly true in disordered systems such as glasses. In contrast to the coupling strength, which is a property that belongs to both the perturbers and the optical center, the fluctuation-rate distribution is usually *intrinsic* to the perturbers themselves, and hence an *intrinsic* property of the host sample. In principle, with proper combination of different dephasing-measurement techniques, the distribution can be mapped out. Thus information about an intrinsic physical property of the sample can be extracted by measuring an extrinsic property, i.e., the dephasing behavior of doped optical centers.

As just discussed, the time scale associated with the two-pulse photon echo is typically on the order of picoseconds to nanoseconds for organic systems and nanoseconds to microseconds for inorganic systems, whereas the waiting time T_W in a hole-burning experiment is typically on the order of minutes. In most cases, however, a major part of the distribution falls into the temporal range between the echo and hole-burning time scales. To map out the fluctuation-rate distribution requires information within this range. This can be accomplished with several existing experimental techniques such as stimulated echoes, accumulated echoes,[5,6] and transient hole burning,[9,15] where the waiting time T_W can be varied continuously through this range.

We previously addressed the issue of using waiting-time-dependent dephasing measurements to probe the fluctuation-rate distributions in a special case of the standard two-level-system (TLS) model of glasses.[12] There, for mathematical simplicity, the fluctuation was treated as a Gaussian-Markoffian stochastic process.[16] In this paper we will present a systematic investigation of the use of line-narrowing techniques to probe the fluctuation-rate distributions in complex systems. In many real systems the localized perturbers can be reasonably modeled as two-level systems. For example, in the TLS model of glasses[17] or spin flips of spin-$\frac{1}{2}$ nuclei in complex crystals,[9] the fluctuations correspond to the transitions between the two levels. Thus we will use a "sudden-jump" model,[18,19] which gives a more realistic description of the fluctuations. A more general discussion, which is independent of the model of the fluctuations, is supplied in Appendix B.

It will be shown that waiting-time-dependent dephasing measurements can indeed be used to reveal the fluctuation-rate distributions, and hence the dynamics in complex systems. A general relation between a waiting-time-dependent dephasing measurement, viz., the stimulated echo, and the fluctuation-rate distribution function of a complex system, regardless of the details of the coupling to the optical center or the spatial distribution of the perturbers, is found to be

$$\frac{\partial \ln(I_S)}{\partial T_W} \propto \int dR\, P_1(R) \exp(-RT_W)\ . \tag{1.1}$$

That is, the derivative of the echo-decay function is

directly proportional to the Laplace transform of the fluctuation-rate distribution function. This result is of central importance. We will demonstrate that analogous relationships for other models of the fluctuations, e.g., Gaussian fluctuations, can also be obtained.

For other waiting-time-dependent dephasing measurements, such as transient hole burning, fluorescence line narrowing, and accumulated echoes, similar relations can readily be established. For example, transient hole burning, the frequency domain equivalent of the stimulated echo, is related to the stimulated-echo decay function through Fourier transform.[11] One can relate the result of a waiting-time-dependent hole-burning measurement to the fluctuation-rate distribution by simply replacing I_s in Eq. (1.1) with the inverse Fourier transform of the hole shapes. Relationships between the results of other experiments and the fluctuation-rate distribution can be established in a similar manner.

II. GENERAL FORMULATION OF THE STIMULATED-ECHO–DECAY FUNCTION

It has been proven previously that coherent nonlinear-optical measurements in disordered systems involving two or three input laser fields can be described in terms of four-point correlation functions.[20] It has also been proven that for optical dephasing measurements, such as two-pulse echoes, accumulated echoes,[11,12] hole burning,[11] and fluorescence line narrowing,[11] the appropriate four-point correlation functions are just variations of the four-point correlation function that describes the stimulated echo. Thus, by developing a proper four-point correlation function for the stimulated echo, we will be able to describe all line-narrowing experiments that are currently in use. This four-point correlation function has been discussed in another context, where it is known as the decay function of the stimulated echo.[16,18,19,21]

Consider a stimulated-echo experiment where the time delay between the second and first pulse is τ, and the delay between the third and second pulse is T_W. The decay of the echo signal is governed by the four-point correlation function[11,12,16,18–21]

$$C(\tau,T_W,\tau)=\left\langle \exp\left[i\sum_j^N \varphi_j(\tau,T_W)\right]\right\rangle , \tag{2.1}$$

$$\varphi_j(\tau,T_W)=\int_0^{\tau}\Delta\omega_j(t)dt-\int_{T_W+\tau}^{T_W+2\tau}\Delta\omega_j(t)dt , \tag{2.1a}$$

where N is the number of the perturbers in the averaging volume V and $\langle\ \rangle$ denotes averages over both the distribution of the perturbers and the history path of the perturbation $\Delta\omega_j(t)$. The latter average is the result of an ensemble average of optical centers.

Many of the aspects of the derivation that involve the sudden-jump model are given in Refs. 18 and 19. Those aspects will only be briefly repeated here.

Assume that the time-dependent frequency modulation $\Delta\omega_j(t)$ originates from sudden jumps between the two levels of the perturbers. The phase perturbation can then be rewritten as[18]

$$\varphi_j(\tau,T_W)=\Delta\omega_j\left[\int_0^{\tau}h(t)dt-\int_{T_W+\tau}^{T_W+2\tau}h(t)dt\right] , \tag{2.1b}$$

where $h(t)$ is a random telegram function that only takes on values of $+1$ and -1. The perturbers are taken to be very weakly coupled with each other, and hence to be statistically *independent*. The total number of perturbers is considered to be large, $N\gg1$. Under these conditions, the correlation function becomes[18]

$$C(\tau,T_W,\tau)=\exp\{-N\langle 1-\exp[i\varphi(\tau,T_W)]\rangle_{H,r,\lambda}\} . \tag{2.2}$$

The averages in the exponent are over the random history path H, the spatial distribution r, and the internal parameters of the perturbers, λ. We have dropped the subindex j since the average over the spatial distribution implys that all perturbers are equivalent.

To describe the dynamic behavior of a sudden-jump two-level perturber, two internal parameters are needed: the energy separation between the levels and the coupling strength to the environment that acts as a heat bath. It is this coupling that causes the sudden jumps between the two levels, which in turn induce the optical dephasing. In most cases the details of the coupling of the perturber to the heat bath can be conveniently replaced by a phenomenological parameter R, the relaxation rate between the two levels towards equilibrium. In simple systems, as considered in Refs. 18 and 19, both the energy separation and the relaxation rate are constant for all perturbers. In complex systems, however, the distributions of both parameters usually span broad ranges.

The averages over space and history have been carried out in Ref. 19. The average over space was carried out first with the assumptions of a uniform spatial distribution of perturbers and a dipole-dipole coupling mechanism between the perturbers and the optical center. It is advantageous to change the sequence of the averages, i.e., to average over history first. This avoids the necessity of imposing the two assumptions and makes the treatment more generally applicable.

Following the procedure employed in Ref. 19, we derive the Laplace transform of the history average,

$$\begin{aligned}\int_0^{\infty}\langle 1-\exp(i\varphi)\rangle_H e^{-\sigma\tau}d\tau &=[1+W_2/(\sigma+2W_1)+W_1/(\sigma+2W_2)]\\ &\quad\times A\{1/k^2-1/[k^2+(2\Delta\omega)^2]\} ,\end{aligned} \tag{2.3}$$

$$k^2=(\sigma+W_1+W_2)^2\frac{\sigma(\sigma+2W_1+2W_2)}{(\sigma+2W_1)(\sigma+2W_2)} , \tag{2.3a}$$

$$\begin{aligned}A=&\frac{2W_1W_2}{(W_1+W_2)^2}\frac{(\sigma+W_1+W_2)^2}{(\sigma+2W_1)(\sigma+2W_2)}\\ &\times(2(W_1+W_2)+\sigma\{1-\exp[-(W_1+W_2)T_W]\}) .\end{aligned} \tag{2.3b}$$

W_1 (W_2) is the transition rate from the lower (upper) to the upper (lower) state. The transition rates are related to the relaxation rate towards equilibrium by $W_1+W_2=R$, subject to the restriction W_1/W_2

$=\exp(-E/kT)$, E being the energy separation between the two levels.

The inverse Laplace transform of Eq. (2.3) is generally of the form

$$\langle 1-\exp(i\varphi)\rangle_H = F_1(R\tau,\Delta\omega\tau;x) + F_2(R\tau,\Delta\omega\tau;x)[1-\exp(-RT_W)] , \quad x=E/2kT , \quad (2.4)$$

where F_1 and F_2 are integral functions. In the limit of $T_W=0$, only the first term on the right-hand side of the equation, F_1, remains nonzero. Thus this term describes the dephasing of the two-pulse echo. It can readily be verified that F_1 goes to zero at $R \gg 1/\tau$ and $R \ll 1/\tau$. This means the two-pulse–echo decay is induced mainly by perturbers whose fluctuation rates are comparable to the measured optical dephasing rate $R \sim 1/\tau$, which is consistent with the qualitative discussion in Sec. I (since, in the two-pulse–echo experiment, the measured dephasing time is of the same order of magnitude as the pulse separation, τ). The temporal behavior of the two-pulse–echo decay is determined by the type of coupling of the optical center to the perturbers, $\Delta\omega(r)$, and the spatial and the relaxation-rate distributions of the perturbers.

The second term of the right-hand side of Eq. (2.4) describes the additional dephasing introduced by the finite waiting time in the stimulated-echo experiment or in other experiments such as hole burning. This additional waiting-time-dependent dephasing term is conventionally referred to as "spectral diffusion."[16,18,19,21] It is caused by slow processes that appear static on the time scale of τ and contribute little to the two-pulse–echo decay. We should point out that for systems in which the inverse of the fluctuation rates continuously span from the two-pulse–echo time scale to considerably slower time scales, the distinction between the two terms is just bookkeeping. There will be rates that contribute to both terms.

The function F_2 is independent of T_W. It determines only the functional form of the stimulated-echo decay arising from spectral diffusion (line shape in a hole-burning experiment), whereas the rate of the echo decay (linewidth) is determined by the factor $1-\exp(-RT_W)$. As discussed in Refs. 16, 18, and 19, when the line shape is Lorentzian and the distribution of relaxation rates is a δ function, $\delta(R-R_0)$, the linewidth is linearly proportional to the factor $1-\exp(-R_0T_W)$ in the long-waiting-time limit $T_W \gg \tau$. When the line shape is not Lorentzian, the linewidth is related to the factor $1-\exp(-RT_W)$ in a more complicated manner.

As a function of the relaxation rate R, F_2 is drastically different from F_1. While falling sharply to zero at $R \sim 1/\tau$, the function $F_2(R\tau,\Delta\omega\tau;x)$ becomes independent of R at $R \ll 1/\tau$, i.e., it approaches a constant in the slow-rate limit. On the other hand, the factor $1-\exp(-RT_W)$ becomes significant only when $T_W \geq 1/R$. Thus the term $F_2(R\tau,\Delta\omega\tau;x)[1-\exp(-RT_W)]$ is a constant in the region $1/\tau > R > 1/T_W$, and it falls quickly to zero at the two limits. This means spectral diffusion is induced mainly by perturbers having inverse fluctuation rates falling in the temporal range between the two-pulse–echo measured dephasing time and the waiting time, $\tau < 1/R < T_W$. In complex systems the fluctuation rates usually span a broad range. Thus, in the long-waiting-time limit $T_W \gg \tau$, the measured dephasing rate can be totally dominated by spectral diffusion.

The windowlike behavior of the term $F_2(R\tau,\Delta\omega\tau;x)[1-\exp(-RT_W)]$ provides us with a fundamentally new, potentially powerful, way of doing spectroscopy. As we have seen, the falling edge at the slow-rate end is governed by the factor $1-\exp(-RT_W)$. Simply by varying T_W we can experimentally vary the number of the perturbers that contribute to the optical dephasing according to their fluctuation rates. Hence we can map out the fluctuation-rate distribution in the sample. We should observe that the dephasing becomes faster (linewidth becomes broader) as the waiting time is increased.

To make the discussion more quantitative, we need to calculate the exact form of the function F_2 in the long-waiting-time limit. From the definition of the Laplace transform, we see that the condition $1/\tau \gg R, 1/T_W$ is equivalent to $\sigma \gg R, 1/T_W$. In this limit the Laplace transform in Eq. (2.3) becomes

$$\{1/\sigma - \sigma/[\sigma^2+(2\Delta\omega)^2]\}/2\,\mathrm{sech}^2(x)[1-\exp(-RT_W)] .$$

The inverse transform is found to be

$$\langle 1-\exp(i\varphi)\rangle_H = \sin^2(\Delta\omega\tau)\,\mathrm{sech}^2(x)[1-\exp(-RT_W)] , \quad (2.5)$$

which implies

$$F_2(R\tau,\Delta\omega\tau;x) = \sin^2(\Delta\omega\tau)\,\mathrm{sech}^2(x), \quad \tau \ll T_W, 1/R . \quad (2.5a)$$

Analysis of the functional behavior of F_2 shows that Eq. (2.5) is an accurate approximation for $1/R \sim T_W \geq 10\tau$. We note that this result can also be derived from a simple two-level rate-equation calculation (see Appendix A).

Thus the four-point correlation function for the long-waiting-time limit is

$$C(\tau,T_W,\tau) = \exp\{-N\langle \sin^2(\Delta\omega\tau)\,\mathrm{sech}^2(E/2kT) \times [1-\exp(-RT_W)]\rangle_{r,\lambda}\} . \quad (2.6)$$

The equation gives a complete description of the decay behavior of a stimulated echo if and only if the time delay between the first two pulses, τ, is much shorter than both the inverse of the fluctuation rates of a large number of perturbers, $1/R$, and the waiting time between the third pulse and the second pulse, T_W. Since, as discussed earlier, all other optical line-narrowing experiments can be described in terms of the correlation function of the stimulated echo, this equation provides a general description of optical dephasing measured by all techniques that involve a waiting time relatively long compared to the dephasing time measured by the two-pulse echo.

It is clear that Eq. (2.6) becomes invalid if the fluctuation rates of all the perturbers fall in the range of

$R \geq 1/\tau$. In this case the exact form of the correlation function is required. A derivation of the exact correlation function, limited to the dipole-dipole coupling and the uniform spatial distribution, can be found in Refs. 18 and 19.

In most complex systems, however, the fluctuation rates of a large portion of the perturbers are in the range $R \leq 1/\tau$. To map out the rate distribution, i.e., to measure the waiting-time dependence of the dephasing rate, one need only focus on the region of $R \sim 1/T_W$. Thus, if the condition $T_W \geq 10\tau$ is satisfied, we can safely use the limiting form of the four-point correlation function, Eq. (2.6). The total amount of optical dephasing induced by perturbers with relatively fast fluctuation rates can be evaluated by extending the validity of Eq. (2.5) to $R \geq 1/10\tau$ by employing a step function that goes to zero at $R = 1/\tau$. When using Eq. (2.6), one should also bear in mind that there is another residual dephasing term that originates from the function $F_1(R\tau, \Delta\omega\tau; x)$ (and from other fast-fluctuation processes such as phonon perturbations). These residual dephasing terms constitute the background of the waiting-time-dependent dephasing-rate measurements. As will be seen, however, this background can be eliminated further by a differential detection scheme.

Derivation of a more explicit form of the correlation function from Eq. (2.6) for specific systems requires knowledge about the form of the coupling between the optical center and the perturbers, and the spatial and internal parameter distributions of the perturbers. Examples of specific systems will be discussed in Sec. IV. In Sec. III we develop a general relation between the waiting-time-dependent dephasing measurements and the fluctuation-rate distribution of the perturbers.

III. PROBING THE FLUCTUATION-RATE DISTRIBUTION

A. Definition of the fluctuation-rate distribution

In general, the average in Eq. (2.6) is in the form of

$$\langle \sin^2(\Delta\omega\tau)\,\mathrm{sech}^2(E/2kT)[1-\exp(-RT_W)]\rangle_{r,\lambda} = \int d\mathbf{r}\,dE\,dR\,P(\mathbf{r},E,R)\sin^2(\Delta\omega\tau) \times \mathrm{sech}^2(E/2kT)[1-\exp(-RT_W)]\,, \tag{3.1}$$

where $P(\mathbf{r},E,R)$ is the probability density of finding a two-level perturber with energy separation E and relaxation rate R at position $\mathbf{r}$. We define the fluctuation rate distribution to be

$$P(R) = A\int d\mathbf{r}\,dE\,P(\mathbf{r},E,R)\sin^2(\Delta\omega\tau)\,\mathrm{sech}^2(E/2kT)\,, \tag{3.1a}$$

where A is a normalization factor. Thus the average can be rewritten as

$$\langle \sin^2(\Delta\omega\tau)\,\mathrm{sech}^2(E/2kT)[1-\exp(-RT_W)]\rangle_{r,\lambda} \propto \int dR\,P(R)[1-\exp(-RT_W)]\,. \tag{3.1b}$$

The physical meaning of the fluctuation-rate distribution $P(R)$ can be interpreted as follows. When the back interaction of the optical center is weak compared with that of the heat bath coupled to the perturbers, the existence of the optical centers has little effect on the dynamics of perturbers, hence internal parameters are independent of $\mathbf{r}$. The average over $\mathbf{r}$ can then be carried out separately and Eq. (3.1) becomes

$$\langle \sin^2(\Delta\omega\tau)\,\mathrm{sech}^2(E/2kT)[1-\exp(-RT_W)]\rangle_{r,\lambda} \propto \int dE\,dR\,P(E,R) \times \mathrm{sech}^2(E/2kT)[1-\exp(-RT_W)]\,. \tag{3.2}$$

Here we have assumed $\Delta\omega$ is only a function of $\mathbf{r}$. We note that both functions $\mathrm{sech}^2(E/2kT)$ and $1-\exp(-RT_W)$ act as cutoffs, the former restricting E to the range $E < 2kT$ and the latter restricting R to the range $R < 1/T_W$. In other words, the optical dephasing is induced only by those perturbers with $E < 2kT$ and $R < 1/T_W$. In conventional temperature-dependence studies, the dephasing rate is measured as a function of temperature at a fixed T_W. This effectively maps out the energy distributions of those perturbers whose relaxation rates are larger than $1/T_W$. Similarly, in our context the fluctuation-rate distribution

$$P(R) = A\int dE\,P(E,R)\,\mathrm{sech}^2(E/2kT) \tag{3.2a}$$

is defined such that it is the average relaxation-rate distribution of those thermally accessible perturbers, i.e., the rate distribution of the *fluctuating* perturbers. In this case, $P(R)$ describes the bulk fluctuations in the sample.

When the back interaction of the optical center is strong, all three variables, $\mathbf{r}$, E, and R, can be correlated. Because the coupling usually is strongly dependent on the distance, the dynamics of the perturbers near an optical center can significantly differ from those of the "distant" perturbers. If the analytic form of the correlation between the spatial positions $\mathbf{r}$ and the other two parameters is known, the spatial average can, in principle, be carried out. If the analytic form of the correlation is unknown, one can still divide the perturbers into finite spatial domains, and consider the perturbers in each domain to be distinct species, with their own fluctuation-rate distribution

$$P_i(R) = A\int dE\,P_i(E,R)\,\mathrm{sech}^2(E/2kT)\,. \tag{3.3a}$$

The optical dephasing is determined by

$$\int dR\left[\sum_i N_i\langle \sin^2(\Delta\omega\tau)\rangle_i P_i(R)\right][1-\exp(-RT_W)]\,, \tag{3.3b}$$

where N_i is the number of perturbers in each domain. The fluctuation-rate distribution, $P(R)$, defined in Eq. (3.1a) now is given by the whole expression inside the large parentheses in Eq. (3.3b). Further discussion about the domain treatment of the correlation between the relaxation rates and the coupling strengths will be given in Sec. IV B. Clearly in this strong-coupling case $P(R)$ only describes the fluctuations actually "seen" by the optical

centers; $P(R)$ can be significantly different from the bulk fluctuations in the sample.

B. Probing the fluctuation-rate distribution

Consider a stimulated echo measured at a series of different waiting times T_W. For each T_W the echo signal is recorded as a function of the delay time between the second and first pulse, τ. The echo signal $I_S(\tau;T_W)$, which will be the central focus in the discussion, is proportional to the four-point correlation function of the stimulated echo (or the stimulated-echo–decay function) developed in Sec. II. We will frequently refer to it simply as the echo-decay function. Since the Fourier transform of the hole spectrum in a hole-burning experiment is proportional to the echo-decay function, in discussing $I_S(\tau;T_W)$ we are also discussing the Fourier transform of the hole spectrum.

In view of our previous discussion, the echo signal $I_S(\tau;T_W)$ varies with the waiting time T_W according to

$$\ln(I_S)\propto-\int_0^{1/\tau}dR\ P(R)[1-\exp(-RT_W)]+\cdots\ , \tag{3.4}$$

where the ellipsis represents contribution of fast fluctuations. Here the fast fluctuations refer to both fluctuations from localized perturbers with $R\geq 1/\tau$ and other perturbations such as coupling to phonons. The population relaxation, i.e., the longitudinal relaxation (T_1) process, has been ignored. An important implication of this equation is that the temporal shape of the decay function does not change with the waiting time if the echo decay is dominated by slow fluctuations.

The derivative of the logarithm of the echo-decay function with respect to T_W, which is a measure of the increase in dephasing rate with increasing waiting time, is given by

$$\begin{aligned}\frac{\partial\ln(I_S)}{\partial T_W}&\propto-\int dR\ P(R)R\exp(-RT_W)\\&=-\int dR\ P_1(R)\exp(-RT_W)\ .\end{aligned} \tag{3.5}$$

From Eq. (3.5) it can be seen that the derivative of the echo-decay function with respect to T_W is insensitive to the background of fast fluctuations. Equation (3.5) also shows a very simple relation between the derivative of the stimulated-echo–decay function and the function $P_1(R)$, namely, the derivative of the natural logarithm of the echo-decay function with respect to T_W is proportional to the Laplace transform of $P_1(R)$.

It is worth noting that the substitute function $P_1(R)$ is the distribution function of the fluctuation rates on a $\ln(R)$ scale,

$$P_1(R)d(\ln R)=P(R)dR\ .$$

In disordered systems, the fluctuation spectra of macroscopic observables are often of the form $1/f$, over a broad range of frequencies f. This implies that the fluctuation-rate distributions are of the form of $1/R$ (see, for example, Ref. 22). This universal feature can be attributed to the fact that fluctuation rates in disordered systems are related to microscopic variables σ by $R\propto e^{-\sigma}$. Even a moderately broad distribution of σ will result in a fluctuation-rate distribution of the form of $1/R$ over several orders of magnitude. The fluctuation-rate distribution on the $\ln(R)$ scale, $P_1(R)$, is directly proportional to the distributions of the underlying microscopic variables. When the fluctuation rate is not related to a microscopic variable in such a manner, the use of $P_1(R)$ should not complicate the mathematical treatment. In the following discussion, we will only consider $P_1(R)$.

If all the nonzero parts of $P_1(R)$ fall within the scan range of T_W, one can, in principle, map out the distribution function by performing an inverse Laplace transform on the derivative of the logarithm of the echo signal with respect to T_W. In a hole-burning experiment, if the hole shape is Lorentzian, the equivalent procedure is to inverse transform the derivative of the hole width with respect to T_W. In those cases where the entire range of $P_1(R)$ cannot be covered, one can select a trial distribution function, perform the Laplace transform, and compare it to the data.

To extend our discussion to the cases other than sudden-jump two-level perturbers, we consider an alternative form of Eq. (3.5),

$$\frac{\partial\ln(I_S)}{\partial\ln(T_W)}\propto-\int d(\ln R)P_1(R)RT_W\exp(-RT_W)\ . \tag{3.6}$$

Letting $u=\ln R$ and $v=\ln(1/T_W)$, we can further reduce Eq. (3.6) to

$$\begin{aligned}&\frac{\partial\ln(I_S)}{\partial\ln(T_W)}\propto-\int du\ P_1(e^u)W(u-v)\ ,\\&W(u)=\exp(u-e^u)\ .\end{aligned} \tag{3.6a}$$

Here again we have a very simple relation between the derivative of the stimulated-echo–decay function and the distribution function $P_1(R)$: the derivative of the natural logarithm of the echo-decay function with respect to $\ln(T_W)$ is proportional to the convolution of $P_1(R)$ and a single-peaked function $W(u)$.

It is interesting to note that $W(u)$ acts in a manner equivalent to an instrument resolution function; in any kind of measurement, the measured signal is always a convolution of the real signal and the resolution of the instrument. For example, the temporal shape of a signal measured by a scanning boxcar integrator is the convolution between the actual temporal shape and the gate width of the boxcar. In analogy, we define $W(u)$ as the "gate function." Clearly, if the variation of distribution function $P_1(e^u)$ is slower than the "gate width," Eq. (3.6a) simply gives

$$\frac{\partial\ln(I_S)}{\partial\ln(T_W)}\propto-P_1(1/T_W)\ . \tag{3.7}$$

Equation (3.6a) is not limited to sudden-jump two-level perturbers. Rather, it can be applied to arbitrary perturbers. The exact form of the gate function differs for different perturbers. In Appendix B we calculate the gate function for perturbers undergoing quasicontinuous motion that can be described by a Gaussian-Markoffian

stochastic process. For dipole-dipole coupling and uniform spatial distribution, the gate function is given by

$$W(u)=\exp(u-e^u)/[1-\exp(-e^u)]^{1/2} . \quad (3.8)$$

We see that this gate function has the same characteristics as that in Eq. (3.6a); both are single peaked about $u=v$, and both have a width $\Delta u \sim \ln(1/T_W)$. Since the sudden jump and the Gaussian processes represent two extreme cases of the nature of the fluctuations of the perturbers, we anticipate that these two common features are universal properties of the gate functions for arbitrary forms of the fluctuations (see Appendix B).

Thus the procedure for obtaining information about the fluctuation-rate distribution is as follows. First, measure the stimulated-echo–decay curve $I_S(\tau;T_W)$ at a series of waiting times T_W. Then take the derivative with respect to $\ln T_W$. If the nature of the perturbers is known, one can use the corresponding gate function to deconvolve Eq. (3.6a) to get the rate distribution. In particular, if the perturbers are two level in nature, the rate distribution function is simply the inverse Laplace transform of Eq. (3.5). If the nature of the perturbers is unknown, a plot of the derivative as a function of $\ln(1/T_W)$ should give the approximate shape of the distribution function. If the distribution function is varying slowly compared to the width of the gate function, the plot is an accurate representation of the distribution function. In Sec. IV we will illustrate the procedures with some concrete examples.

IV. APPLICATIONS

To apply the technique described in Sec. III we need to further develop the correlation function in Eq. (2.6). For a particular system, this requires knowledge of the spatial and the internal parameter distributions of the perturbers and the form of the coupling between the optical center and the perturbers. The two most common cases in the condensed-matter systems, i.e., glasses that can be treated as continuous media and complex crystals that consist of discrete lattices, are considered. Other complex systems, such as proteins, could be handled in an analogous manner.

At low temperatures, in both glass and complex crystal systems, optical dephasing is induced predominantly by the slow fluctuations. In glasses, the fluctuations are caused by the varying local structural configurations, which are generally described by the two-level–system model.[17,23] This model has been successful in elucidating physical properties of glasses, such as their low-temperature heat capacities.[17,24] The fluctuation-rate distribution varies continuously over a broad range. Measurements on chromophores in glasses have found that the results of spectral hole-burning and two-pulse photon-echo experiments differ significantly.[10,11] Until recently, the spectrum of the hole was considered to be the Fourier transform of the echo decay. In fact, the dephasing rates obtained from the widths of the holes are found to be significantly larger than those measured with the photon echo. In light of the developments given in the preceding sections, this is as expected. The authors of Ref. 11 analyzed both experiments and presented a correct description of the fundamental difference between these two experiments, and other line-narrowing experiments, based on the dependence of the experimental observables on T_W. Using the simplest TLS model of glasses [$P(R)=1/R$ for all R], they were able to explain the observed differences between the hole burning and echo experiments semiquantitatively.

In crystals with paramagnetic optical centers, the fluctuations can be caused by the flipping of electronic or nuclear spins of the host lattice (or of the depant, if the concentration is sufficiently high).[9,25] When the coupling between the optical center and the surrounding spins is weak, the flip rate is usually a constant, i.e., the distribution is a δ function (several δ functions if more than one species of spins exist). In this case, the flip rate is just a property of the pure host lattice. The flip rate can be severely affected, however, by an external field. Thus the free bulk flip rate may not be readily measured with standard spin-resonance techniques.

When the coupling between the optical center and the host spins is strong, the dynamics of the spins is affected by the existence of the optical center.[9] The strong coupling detunes the spins from the bulk resonance frequency and hence slows down their flip rates. The greater the coupling strength, the slower the flip rate. Since the coupling strength is dependent on the distance between a spin and the optical center, the flip rates are distributed over a broad range. In this case, the distribution is in the form of many peaks, because of the discrete nature of the system. As in glasses, two-pulse–echo and hole-burning dephasing measurements have been observed to differ significantly in such complex crystals.[9]

We note that the fluctuation-rate distribution in complex crystals is extrinsic, i.e., it is introduced by the optical center. In contrast, the fluctuation-rate distribution in a glass is essentially intrinsic. It is a bulk property of the glass, although recent experiments suggest that the rate distribution may also be modified by the perturbers' coupling to the optical center.[26]

A. Stimulated-echo–decay function in glasses

In glasses, it is reasonable to assume that the perturbers are uniformly distributed over space, i.e.,

$$P(\mathbf{r})d\mathbf{r}=dV/V ,$$

where $\mathbf{r}$ is the position relative to the optical center. The interaction between a perturber and an optical center has been proposed to be dipole-dipole in nature. The coupling could be of an electric dipole of a localized perturber to the permanent electric dipoles of the ground and excited states of the optical center, or it could be an "elastic dipole" induced by the perturber that produces a strain field at the optical center which couples to the electronic states of the center.[23,27] The dipolar coupling mechanism is consistent with the TLS model. It has support from a variety of experiments.[23] Therefore, we will assume the interaction has the form of dipole-dipole coupling, $\Delta\omega=\eta/r^3$.

For simplicity, we also assume that the backinteraction

of the optical center can be ignored. Thus the internal parameters of a TLS are considered to be uncorrelated with its distance to or its coupling strength with the optical center. Using these assumptions and making the substitution $\eta\tau/r^3=x$, we can perform the spatial average in Eq. (2.6). The four-point correlation function then becomes

$$C(\tau,T_W,\tau)=\exp\{-\alpha\tau\langle\bar{\eta}\,\mathrm{sech}^2(E/2kT)\times[1-\exp(-RT_W)]\rangle_\lambda\}\ ,\qquad \alpha=(2\pi^2/3)(N/V)\ , \tag{4.1}$$

where $\bar{\eta}$ is the coupling constant averaged over the relative orientations of the perturbers,

$$\bar{\eta}=\langle|\eta|\rangle_\theta\ .$$

The relation

$$\int_0^\infty \frac{\sin^2(x)dx}{x^2}=\frac{\pi}{2}$$

is also used in the derivation. We note that this result is essentially identical to that given in Ref. 28.

From Eq. (4.1) we see that the decay function of the stimulated echo at long waiting time $T_W\gg\tau$ is *always exponential*. The finite waiting time adds a waiting-time-dependent factor $1-\exp(-RT_W)$ to the echo-decay rate, i.e., spectral diffusion increases the decay rate (increases the linewidth) according to $\langle 1-\exp(-RT_W)\rangle_\lambda$. Note that we are working in the limit $T_W\gg\tau$. The spectral diffusion contribution is *not* governed by this factor for very short waiting times.

We emphasize that the exponential decay is solely a result of a uniform distribution of dipolelike perturbers, independent of the details of the internal parameter distributions of the perturbers. Since the four-point correlation function that describes the hole-burning signal is just the Fourier transform of the stimulated-echo four-point correlation function,[11] the fact that all the hole shapes so far observed in glasses are Lorentzian is very convincing evidence that the interaction between the perturbers and the chromophores in glasses is dipole-dipole.[23]

That a Lorentzian line shape is related to uniformly distributed dipolelike perturbers was first realized in the analysis of spin-resonance experiments (see, e.g., Refs. 16, 18, 19, and 21). It has been applied to the analysis of optical dephasing measurements by many authors (see, e.g., Refs. 11 and 27). However, it should be pointed out that this conclusion only applies to line shapes measured in the long-waiting-time limit $T_W\gg\tau$. Without detailed knowledge about the internal parameter distributions of the perturbers, one cannot reach any conclusion about the functional form of the decay of a two-pulse echo. The observed exponential decays in two-pulse–echo experiments, which correspond to Lorentzian line shapes, require a fluctuation-rate distribution proportional to $1/R$ for rates on the order of $1/\tau$ in addition to the uniform spatial distribution of dipolelike perturbers.[11,12,29]

B. Probing the fluctuation-rate distribution in glasses

At low temperature ($T\sim 1$ K) it is found that two-pulse photon-echo signals decay exponentially in the temporal range from ~ 10 ps to a few nanoseconds in some organic glasses,[11,12] and from ns to μs in an inorganic glass.[30] These experimental results can be related to a fluctuation-rate distribution that is inversely proportional to the rate itself, $P(R)\sim 1/R$, or alternatively, $P_1(R)=$const, for rates that are on the order of the inverse of these temporal ranges. The behavior of $P_1(R)$ at slower rates, $R<\mu\mathrm{s}^{-1}$, is unclear, but it is logical to believe that $P_1(R)$ should fall to zero at some minimum rate $R_{\min}$; otherwise the total power of the fluctuations would become infinite.

In recent experiments performed on resorufin in ethanol and *d*-ethanol glasses,[10,11,26] it was found that dephasing rate measured with hole burning is a factor of 6 larger than that measured with two-pulse–echo experiments. Analysis of the data using the standard tunneling TLS model indicates $R_{\min}$ to be on the order of ms^{-1} in these systems.[12,26] Thus, if an experiment is performed as described above, with the waiting time T_W scanned in the range of milliseconds, it should be possible to map out the falling edge of the rate distribution in these glasses.

The behavior of $P_1(R)$ at $R>(10\ \mathrm{ps})^{-1}$ is unknown. However, our discussion is not affected by this detail, for the derivative of the stimulated-echo–decay function is independent of the fast fluctuations. Thus it is sufficient to assume that the distribution goes to zero at some maximum cutoff rate $R_{\max}\gg 1/T_W$.

Following the analysis in Sec. III we rewrite Eq. (4.1) as

$$C(\tau,T_W,\tau)=\exp\left[-\beta\tau\int d(\ln R)P_1(R)\times[1-\exp(-RT_W)]\right]\ , \tag{4.2}$$

where β is the product of α and a collection of constants that arise from the energy average. The actual form of the distribution is determined by the nature of the perturbers.

Assume the perturbers can be described by the tunneling TLS model. Using the same procedure as that in Ref. 12, we find

$$\beta\propto\alpha(kT)^{1+\mu} \tag{4.2a}$$

and

$$P_1(R)\propto\int_{x_{\min}}^\infty dx\,x^\mu\,\mathrm{sech}^2(x/2) \tag{4.2b}$$

in the range $R>R_{\min}$, where $x_{\min}=2[R/R_{\max}(2kT)]^{1/2}$, $R_{\min}$ is determined by maximum possible value of the tunneling parameter, and, as we discussed above, $R_{\max}(2kT)>(10\ \mathrm{ps})^{-1}$. In this model the distribution of energy separations is assumed to be $P(E)\propto E^\mu$ with a cutoff at $E=E_{\max}\gg kT$. Experimental results suggest that the exponent μ takes on a value between 0 and 1.[23]

From Eq. (4.2b) it can be seen that for slow fluctuation rates, $R\ll R_{\max}(2kT)$, $P_1(R)$ is essentially independent of R. Thus in the range we are interested in, from $\mu\mathrm{s}^{-1}$

to ms^{-1}, the distribution can be taken to be a constant. It is unlikely, however, that $P_1(R)$ falls to zero instantaneously at R_{min}. In reality, the nature of $P_1(R)$ near R_{min} could behave in various ways. Using waiting-time-dependent dephasing measurements, it should be possible to probe the actual behavior of the distribution.

Consider some examples.

(1) The distribution suddenly goes to zero at R_{min},

$$P_1(R)=AH(R_{max}-R)H(R-R_{min}) , \tag{4.3}$$

where A is a normalization factor, $A=\ln(R_{max}/R_{min})$. The derivative of the stimulated-echo–decay function on a logarithmic scale, according to Eq. (3.3), is found to be proportional to

$$\frac{\partial \ln(I_S)}{\partial \ln T_W} \propto A \exp(-R_{min}T_W) . \tag{4.3a}$$

One can indeed derive a distribution function by performing an inverse Laplace transform of Eq. (4.3a). The result is

$$P_1(R)=AH(R-R_{min}) . \tag{4.3b}$$

The first step function, $H(R_{max}-R)$, does not appear in Eq. (4.3b). This is not surprising because it was assumed that $R_{max}\gg 1/T_W$, which is equivalent to letting R_{max} be infinite.

(2) The distribution falls to zero as a Gaussian function,

$$P_1(R)=A(H(R_{max}-R)H(R-R_0) + H(R_0-R)\exp\{-[\ln(R/R_0)/\sigma]^2\}) , \tag{4.4}$$

where $R_0>R_{min}$, and σ is given by

$$\sigma=(2/\sqrt{\pi})\ln(R_0/R_{min}) .$$

All the parameters have the same values as that in Eq. (4.3). σ and R_0 are chosen in such a way that the total area covered by this distribution is the same as that covered by the step-function distribution in Eq. (4.3). We note that the Gaussian here refers to a Gaussian function on the $\ln R$ scale. The derivative of the decay function is found to be proportional to

$$\frac{\partial \ln(I_S)}{\partial \ln T_W} \propto \frac{2A}{\sigma^2}\int_0^\infty du\, u \exp[-R_0T_We^{-u}-(u/\sigma)^2] , \tag{4.4a}$$

where $u=-\ln(R/R_0)$.

(3) The distribution falls to zero exponentially,

$$P_1(R)=A\{H(R_{max}-R)H(R-R_0) + H(R_0-R)\exp[\ln(R/R_0)/\sigma]\} , \tag{4.5}$$

where $\sigma=\ln(R_0/R_{min})$, and all other parameters have the same values as that in Eq. (4.4). With these parameters, the area covered by this distribution is the same as in cases 1 and 2. The derivative of the corresponding decay function is given by

$$\frac{\partial \ln(I_S)}{\partial \ln T_W} \propto \frac{A}{\sigma}\int_0^\infty du \exp(-R_0T_We^{-u}-u/\sigma) . \tag{4.6}$$

All three distribution functions are plotted in Fig. 1. The parameters used in the plot are $R_{max}=10^{11}\ s^{-1}$, $R_{min}=10^3\ s^{-1}$, and $R_0=10^5\ s^{-1}$. As a reference, we also plot the function $1-\exp(-RT_W)$ and the gate function $RT_W\exp(-RT_W)$ at fixed waiting times $T_W=10\ \mu s$, showing the effect of scanning T_W. The time delay between the first two pulses is assumed to satisfy the condition $T_W/\tau\gg 1$. The echo-signal–decay rate is proportional to the area under the function, $1-\exp(-RT_W)$. At a particular T_W, the rate of increase with T_W of the echo-signal–decay rate is proportional to the area under the gate function.

In Fig. 2(a) the value of $\langle 1-\exp(-RT_W)\rangle_R$, which is proportional to the decay rate of the echo signal, is plotted as a function of T_W. It can be seen from the plot that in the short-waiting-time limit $T_W\ll 1/R_{min}$, $\langle 1-\exp(-RT_W)\rangle_R$, the echo-decay rate, increases in proportion to the logarithmic time scale. In the long-waiting-time limit $T_W\gg 1/R_{min}$, $\langle 1-\exp(-RT_W)\rangle_R$ approaches a constant value, regardless of the functional form of $P_1(R)$ near R_{min}. Thus if one measures the dephasing rate in the long-waiting-time limit, as is the case in most persistent hole-burning experiments, the measured dephasing rate is determined by the total area covered by the distribution function and does not reflect the details of the fluctuation-rate distribution. Further-

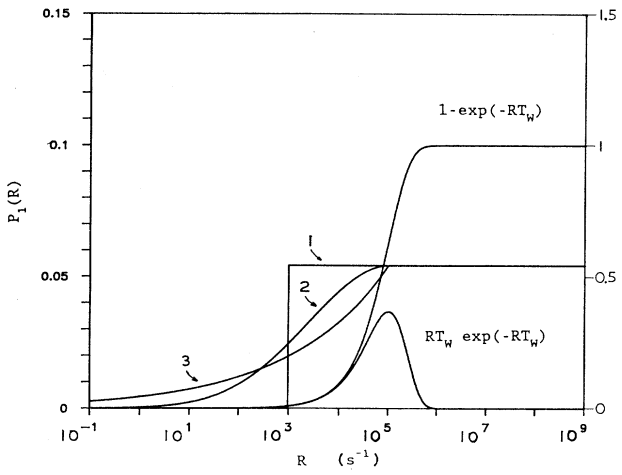

FIG. 1. Model fluctuation-rate distributions $P_1(R)$ for a glass (left-hand scale). The cutoffs at the low fluctuation rates are assumed to be 1, a step function; 2, a Gaussian function; and 3, an exponential function (see text). The parameters used in the plot are $R_{max}=10^{11}\ s^{-1}$, $R_{min}=10^3\ s^{-1}$, and $R_0=10^5\ s^{-1}$. As a reference, we also plot the function $1-\exp(-RT_W)$ and the gate function $RT_W\exp(-RT_W)$ at fixed waiting times $T_W=10\ \mu s$, showing the effect of scanning T_W (right-hand scale). The echo-signal–decay rate is proportional to the area under the function, $1-\exp(-RT_W)$. At a particular T_W, the rate of increase with T_W of the echo-signal–decay rate is proportional to the area under the gate function.

more, if T_W is varied, but always kept in the $T_W \gg 1/R_{\min}$ range, the measured dephasing rate will be independent of T_W.

In Fig. 2(b) the derivative with respect to $\ln T_W$ of the average of the function $1-\exp(-RT_W)$, i.e., the convolution of the distributions with the gate function, $\langle RT_W \exp(-RT_W)\rangle_R$, is plotted as a function of T_W. This plot is the change of the measured dephasing rate versus waiting time T_W. The manifestations of the differences in the distributions are much clearer than in Fig. 2(a). In all three cases, at short waiting time $T_W \ll 1/R_{\min}$, the change of the echo dephasing rate is a constant. At long waiting time $T_W \gg 1/R_{\min}$, the change in the dephasing rate becomes zero. As T_W is scanned through the region $(1/R_0, 1/R_{\min})$, a transition between these two limiting values occurs. The functional form of the transition is determined by the nature of the distribution function. The results for the three different distributions are clearly distinguishable.

In Fig. 2(c), Fig. 2(b) is replotted using a $1/T_W$ scale. With this scale, the derivatives of the echo-decay rates closely resemble the corresponding fluctuation-rate distributions. If the rate distribution falls off relatively slowly, as in curves 2 and 3, the data are essentially the

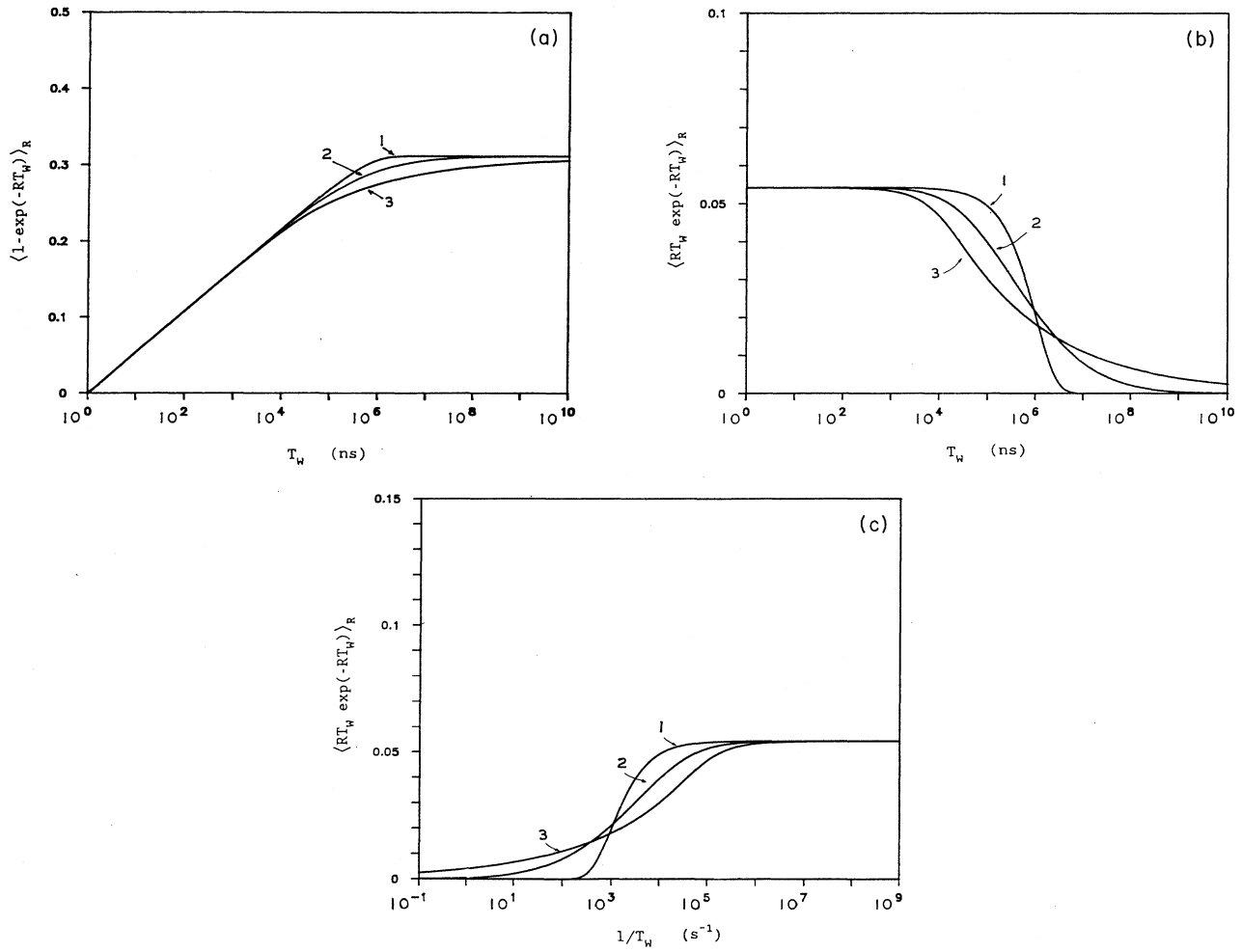

FIG. 2. (a) Plot of $\langle 1-\exp(-RT_W)\rangle_R$ as a function of T_W. The distribution functions used in the averages are those plotted in Fig. 1. This plot is equivalent to the dephasing rate measured by the stimulated echo (or hole burning) vs the waiting time T_W. Curve 1: step-function distribution. Curve 2: Gaussian distribution. Curve 3: exponential distribution. (b) Plot of $\langle RT_W \exp(-RT_W)\rangle_R$ as a function of T_W. This plot is equivalent to the derivative of the stimulated-echo–decay rate (derivative of the hole width) vs the waiting time T_W. The influence of the different distributions on the echo signal is much clearer. When T_W is short, the derivative of the decay rate is a constant. When T_W is in the region of the cutoff in the rate distribution, the derivative is changing rapidly. When T_W is long, the derivative goes to zero, i.e., the echo-decay rate (hole width) no longer changes with increasing T_W. (c) (b) is replotted on a $1/T_W$ scale. Note the similarity between this plot and the corresponding fluctuation-rate distributions in Fig. 1. If the rate distribution falls off relatively slowly, the data are essentially the fluctuation-rate distribution. Only curve 1, the step-function distribution, shows appreciable modification of the underlying rate distribution function.

fluctuation-rate distribution. Only curve 1, the step-function distribution, shows appreciable modification of the underlying rate distribution function.

Besides the functional behavior of the fluctuation-rate distribution, the technique can reveal the temperature dependence of the cutoff rate $R_{\min}$. Using the standard TLS model, we find that the cutoff fluctuation rate is given by[12]

$$R_{\min}=2kT\Omega(\Delta_{0,\min})^2 , \tag{4.7}$$

where Δ_0 is the coupling strength, or the tunneling rate, between the two potential wells of the TLS, and Ω is a collection of constants describing the coupling between the TLS and the acoustic-phonon heat bath.[24] Thus one would expect $R_{\min}$ to be linearly related to the temperature. There are factors, however, which could make the temperature dependence more complicated.

One obvious factor would be the breakdown of the TLS model. This is beyond the scope of the current discussion. Within the framework of the TLS model, it is still possible for the cutoff rate to display a nonlinear temperature dependence. For example, Eq. (4.7) is derived with the Debye approximation, i.e., the phonon density of states is proportional to the square of the frequency. It is believed that this is an accurate approximation at $T<1$ K.[17,24] There is no experimental evidence, however, showing that this approximation is still valid above 1 K. Thus it should be possible to gain significant insight into the dynamics in glasses by measuring the temperature dependence of $R_{\min}$.

Furthermore, there is a one-to-one correspondence between the experimental variables $[T,T_W]$ and the internal parameters of the TLS $[E,R]$. If the relaxation mechanism of the TLS is known, e.g., single-acoustic-phonon absorption and emission, $[E,R]$ can be expressed in the two-dimensional space of the tunneling rate and the asymmetry of the TLS, $[\Delta_0,\Delta]$. Therefore, in principle, it should be possible to map out the distributions of both the tunneling rates and the asymmetries of the TLS by doing waiting-time-dependent dephasing measurements at different temperatures.

We should point out that the experimental approach discussed here is related in spirit to the time-dependent specific-heat measurements originally proposed by Black *et al.*[28] The idea behind the time-dependent specific-heat measurement is that those TLS's with relaxation rates slower than the time scale of the measurement do not contribute to the measured specific heat. Thus the specific heat of an amorphous material should increase with time. Several experimental studies have been published on this subject.[31–33] Because of intrinsic problems related to the specific-heat measurements, such as nonuniform heating and finite thermal diffusion rates, however, the time scale of the experiments are limited to tens of milliseconds or longer. The results at shorter times are inconclusive.

C. Stimulated-echo–decay function in complex crystals

In crystals, the perturbers are restricted to points on the host lattice. The spatial distribution function is

$$P(\mathbf{r})=(1/N)\sum_j \delta(\mathbf{r}-\mathbf{r}_j) ,$$

where $\mathbf{r}_j$ is a possible position of a perturber relative to the optical center. The $\mathbf{r}_j$ are determined by the crystal lattice structure.

If the correlation between the coupling strength of the optical center to the host perturbers and the perturbers' jump rates can be ignored, the four-point correlation function becomes

$$C(\tau,T_W,\tau)=\exp\left[-\sum_j \sin^2[\Delta\omega(\mathbf{r}_j)\tau]\times\langle \mathrm{sech}^2(E/2kT)\times[1-\exp(-RT_W)]\rangle_\lambda\right] . \tag{4.8}$$

This situation would be encountered in the limit of weak coupling.

If the coupling is so weak that $\Delta\omega(\mathbf{r}_j)\tau\ll 1$, i.e., the modulation frequencies of all the perturbers are smaller than the optical dephasing rate, Eq. (4.8) yields a Gaussian decay function. This conclusion only requires the condition of weak coupling. It does not rely on the assumption of a Gaussian stochastic process, as has been suggested by many authors. We also see that the broadening of the linewidth (increase in the dephasing rate over that measured with a two-pulse echo) goes as $[1-\exp(-RT_W)]^{1/2}$. This is in contrast to the results obtained for glasses discussed above.

If the coupling of the perturbers to the optical center is strong and the correlation between the coupling strength and the jump rate cannot be ignored, one can, in principle, follow the argument in Sec. III A to decouple the correlation. As will be seen, however, it is often sufficient to use a few discrete rates assigned to certain groups of perturbers in a practical calculation.

In Sec. IV D experimental results from a complex crystal are analyzed. The perturbers are spin-$\frac{1}{2}$ F nuclear spins and the fluctuations involve spin flips. Since data are available and spin dynamics are relatively well understood, this example provides a concrete demonstration of the theory.

D. Analysis of Pr^{3+}:CaF_2 transient hole-burning measurements

In this subsection we consider a set of elegant low-temperature ($T\sim 2$ K) optical dephasing measurements performed on a Pr^{3+}:CaF_2 crystals by Shelby and MacFarlane.[9] The experiment was performed on the $^1D_2$-$^3H_4$ (594.1 nm) optical transition of the Pr^{3+} ions. It was found that the two-pulse photon echo measures a dephasing rate that corresponds to a homogeneous width of 370 kHz, whereas persistent hole burning measures a hole width of 9 MHz.[9] Shelby and MacFarlane pointed out that the difference is caused by spectral diffusion induced by the relatively slow (compared to the optical dephasing time) spin flips of F^- nuclei. In bulk LaF_3 crystals the flip rate is $(170\ \mu s)^{-1}$.[34] Because of similarities

between LaF_3 and CaF_2 crystals, it is believed that the spin-flip rate in bulk CaF_2 should be of the same order, i.e., about several kHz.

To support the qualitative explanation of spectral diffusion as the source of the difference between the echo and hole-burning results, Shelby and MacFarlane performed a transient hole-burning experiment using the technique of delayed optical free-induction decay (FID). In the experiment, a narrow saturation hole is generated in the inhomogeneously broadened optical line by a laser pulse having a duration of a few microseconds. After a delay time T_W, a short probe pulse ($\sim 50-100$ ns) is applied to induce the optical FID. The signal is heterodyne detected, i.e., the E field generated by the decaying FID macroscopic polarization is detected. It is found that dephasing rate of the delayed FID signal, which is related to the width of the hole, increases with the delay time T_W from 1 MHz at $T_W=1$ μs to 6 MHz at $T_W=5$ ms. Although not interpreted quantitatively, these measurements give very strong support to the proposed spectral diffusion model of the hole broadening.

Using the theoretical technique developed in the preceding sections, we analyze the experiment more quantitatively as follows. Let the preparation (burning) pulse be a square pulse with a duration Δt, and the probe (reading) pulse be a δ function $\delta(\tau)$, where $\tau=t-(T_W+\Delta t)$ is the time relative to the probe pulse. Neglecting radiative decay of the excited state, we find that the FID signal decays as a function of τ according to (see, for example, Ref. 12)

$$\int_{T_W}^{T_W+\Delta t-\tau} dt_2 C(\tau,t_2,\tau)\rightarrow C(\tau,T_W,\tau)\ , \quad T_W \gg \Delta t,\tau\ . \tag{4.9}$$

This is the same four-point correlation function that describes the decay of the stimulated echo.

The dominant part of the time-dependent perturbation responsible for optical dephasing is from the magnetic dipole-dipole coupling between the nuclear spins of surrounding F^- ions and the strong ground-state magnetic moment ($g=5.45$ MHz/G) of the Pr^{3+} ion.[35] The excited-state magnetic moment of the Pr^{3+} ion is 3 orders of magnitude weaker.

The flipping of a F^- nuclear spin is induced by cross relaxations[36] with neighboring F^- nuclear spins. If F^- spins are aligned with the strong local field produced by the Pr^{3+} ion, the coupling strength $\Delta\omega(\mathbf{r}_j)$, is given by the point dipole-dipole interaction

$$\Delta\omega(\mathbf{r}_j)=|\boldsymbol{\mu}_j|\,|\boldsymbol{\mu}_A-3\mathbf{r}_j(\boldsymbol{\mu}_A\cdot\mathbf{r}_j)/r_j^2|/r_j^3\ , \tag{4.10}$$

where $\boldsymbol{\mu}_j$ and $\boldsymbol{\mu}_A$ are the magnetic moments of the F^- nuclear spin and the ground state of the Pr^{3+} ion, respectively.

Thus, if the four-point correlation function given by Eq. (4.8) is strictly applicable, we would be led to a straightforward result. In this case, however, the situation is more complex. The complication is caused by the strong ground-state magnetic moment of the Pr^{3+} ion.

When a Pr^{3+} ion is in the excited state, the nuclear spins of all the surrounding F^- ions flip freely at a single rate R_0 of several kHz, i.e., the F^- nuclear spins flip at the same rate as in the bulk crystal and have a rate distribution of $\delta(R-R_0)$. When a Pr^{3+} ion is in the ground state, however, its magnetic moment generates a large local field that detunes the nuclear spins of nearby F^- ions from the bulk F^- nuclear-spin resonance. This drastically reduces the flipping rate of the closest spins and generates what has been called a "frozen core."[9,35] In other words, when a Pr^{3+} ions is in the ground state the fluctuation rates of the surrounding F^- nuclear spins are correlated with the coupling strength: the weaker the coupling, the larger the rate. Therefore, the fluctuation rates are correlated with the positions of the F^- ions relative to the Pr^{3+} ion, since the relative positions determine the coupling strength.

In addition to the differences in the fluctuation-rate distributions when Pr^{3+} is in its ground and excited states, the coupling strengths are also different. If a Pr^{3+} ion is the ground state, the surrounding F^- spins are aligned with the strong local field generated by the Pr^{3+} large magnetic moment. If a Pr^{3+} ion is the excited state, the surrounding F^- spins are oriented randomly. Randon orientation produces, on average, weaker coupling.

Equation (4.8) was written with the assumption that there is no correlation between the flip rate and the coupling strength. The physical factors discussed above indicate that Eq. (4.8) is not a complete description for the Pr^{3+}:CaF_2 situation.

We tackle this problem by noting that the delayed FID signal actually originates from two groups of P^{3+} ions: those that form a "hole" in the ground state and those that form an "antihole" in the excited state. First consider the limit of $T_W \ll T_0$, where $T_0=509$ μs is the lifetime of the excited state. With $T_W \ll T_0$, the P^{3+} ions do not change their states during the waiting time. From the above discussion, we see that the four-point correlation function should be divided into two parts,

$$C(\tau,T_W,\tau)=C_G(\tau,T_W,\tau)+C_E(\tau,T_W,\tau)\ , \tag{4.11}$$

where $C_G(\tau,T_W,\tau)$ describes the dephasing of the Pr^{3+} ions in the ground state and $C_E(\tau,T_W,\tau)$ describes the dephasing of the Pr^{3+} ions in the excited state.

In the long-waiting-time limit $T_W \gg T_0$, most excited-state Pr^{3+} ions have returned to the ground state through radiative decay. If $C_G(\tau,T_W,\tau)$ and $C_E(\tau,T_W,\tau)$ were identical, the antihole in the excited state would fill the hole in the ground state as the excited states decay, and the FID signal would disappear. Because the flip rates of the surrounding spins are much faster when a Pr^{3+} ion is in the excited state, and, therefore, the antihole is being broadened much faster than the hole, most excited-state Pr^{3+} ions relax to the wings of the hole. This leaves a persistent hole in the ground-state population. Thus the persistent hole observed in this system is a combined effect of the time evolutions of both states.

In the time-domain description, the signal generated by the Pr^{3+} ions that were in the excited state and have returned to the ground state destructively interferes with the signal generated by those ions that remained in the ground state. If all of the ions in the excited state sud-

denly returned to the ground state at a single time T_0, the correlation function describing the FID signal for times longer than T_0 is given by

$$C(\tau,T_W,\tau)=C_G(\tau,T_W,\tau)-C_{EG}(\tau,T_W,\tau;T_0)\ , \tag{4.12}$$

where $C_{EG}(\tau,T_W,\tau)$ describes the dephasing of the Pr^{3+} ions that were originally in the excited state and returned to the ground state at T_0.

Combining Eqs. (4.12) and (4.11), and including the exponential decay of the excited-state population, the general form of the correlation function for arbitrary waiting time T_W is

$$C(\tau,T_W,\tau)=C_G(\tau,T_W,\tau)+\exp(-T_W/T_0)C_E(\tau,T_W,\tau)-\frac{1}{T_0}\int_0^{T_W}dt\,\exp(-t/T_0)C_{EG}(\tau,T_W,\tau;t)\ . \tag{4.13}$$

The first term in Eq. (4.13) represents the contribution to the FID from ground-state ions that were never excited. The second term is the contribution from excited-state ions. The contribution from this term decays exponentially at rate $1/T_0$ as the ions return to the ground state. The third term arises from ions that have returned to the ground state after being excited.

Using a rate-equation calculation (see Appendix C), we find that the four-point correlation functions corresponding to the three different groups of Pr^{3+} ions are

$$C_G(\tau,T_W,\tau)=\exp\left[-\sum_j \sin^2(\Delta\omega_j\tau)[1-\exp(-R_jT_W)]\right]\ , \tag{4.13a}$$

$$C_E(\tau,T_W,\tau)=\exp\left[-\frac{1}{2}\sum_j [1-\sin(2\Delta\omega_j\tau)/2\Delta\omega_j\tau][1-\exp(-R_0T_W)] + \{\sin(2\Delta\omega_j\tau)/2\Delta\omega_j\tau-[\sin(\Delta\omega_j\tau)/\Delta\omega_j\tau]^2\}R_0T_W\exp(-R_0T_W)\right]\ , \tag{4.13b}$$

$$C_{EG}(\tau,T_W,\tau;t)=\exp\left[-\sum_j \sin^2(\Delta\omega_j\tau)\{1-\exp[-R_0t+R_j(T_W-t)]\}\right]\ . \tag{4.13c}$$

In deriving Eq. (4.13), we have set $\mathrm{sech}^2(E/2kT)=1$, since the energy separations of the F^- nuclear spins are orders of magnitude smaller than the thermal energy at the experimental temperature $T\sim 2$ K. It was also assumed that the local field at each spin site is dominated by the dipole field induced by the Pr^{3+} ion when the latter is in the ground state, but points in a random direction when the Pr^{3+} ion is in the excited state. The coupling strength in Eq. (4.13b) has been averaged over the random orientations of the spins with respect to the direction of the dipole field.

In the excited-state correlation function $C_E(\tau,T_W,\tau)$, the fluctuation of the spins is described by the single bulk spin-flip rate, i.e., the fluctuation-rate distribution of the spins is a δ function, $P(R)=\delta(R-R_0)$. In the correlation functions $C_G(\tau,T_W,\tau)$ and $C_{EG}(\tau,T_W,\tau;t)$ a fluctuation rate R_j is associated with each spin since the fluctuation rates of spins surrounding a ground-state Pr^{3+} ion are correlated to the spin positions.

In principle, R_j should span quasicontinuously from the fastest bulk rate R_0 to some slowest rate associated with those F^- spins that are coupled most strongly to the Pr^{3+} ion, i.e., the interstitial or the nearest-neighbor F^- spins. Experimentally, the flip rate of the nearest-neighbor spins is found to be on the order of s^{-1}.[9] It has been proposed that these slow flips are responsible for the persistent hole burning.[9,35]

Because the form of the correlation between the flip rate R_j and the coupling strength is unknown, we divide the spins into three groups to make the calculation manageable. When the Pr^{3+} ion is in its ground state, the flip rates of the spins within each group can be approximated by a single rate. (1) The interstitial and the nearest-neighbor F^- spins' flip rates are taken to be zero, because the maximum waiting time in the experiment, 5 ms, is several orders of magnitude shorter than the inverse of these flip rate [$\sim(s)^{-1}$]. (2) The F^- spins far away from the Pr^{3+}-ion flip rates are taken to be the same as the free bulk rate R_0 [$\sim(ms)^{-1}$]. (3) The F^- spins at intermediate distances flip rates are slower than R_0 but still significant on the experimental time scale. Because of the limited amount of data and for simplicity, we assume that the flip rates of this group can be replaced by a single rate R_1. We set the close-in boundary of this last group of spins to be the second-nearest neighbors. The outer boundary is found in the fitting process to be somewhere between the fourth- and seventh-nearest neighbors.

When the Pr^{3+} ion is in the excited state, all the spins are assumed to have the bulk flip rate R_0. Thus in this model, the rate distribution is composed of two δ functions, the rates R_0 and R_1. Fitting the data yields the values of these two rates.

In Fig. 3, Eq. (4.13) was fitted to the raw experimental results provided to us by the authors of Ref. 9. In analogy to the conventional definition of $2/\pi T_2$ as the hole width in the absence of localized fluctuations, the vertical axis is chosen to be $1/\pi\tau_e$, where τ_e is the time at which the FID signal has decayed to the $1/e$ point (note that the dephasing time T_2 is defined to be $T_2=2\tau_e$). The horizontal axis is the waiting time T_W.

The fitting procedure is as follows. First, we notice that in the data the hole width increases steadily with waiting time in the range $T_W<0.1$ ms. This increase

arises from the free spin flips at R_0 that cause excited-state spectral diffusion and, to some extent, ground-state spectral diffusion. The contribution of the spin flips at the slower rate R_1 is negligible at short times. Around $T_W = 0.5$ ms, there is a bump in the data. In view of the qualitative discussion given above, this is the result of the competition between line broadening and population decay of the excited Pr^{3+} ions since the lifetime is $T_0 = 509$ μs.

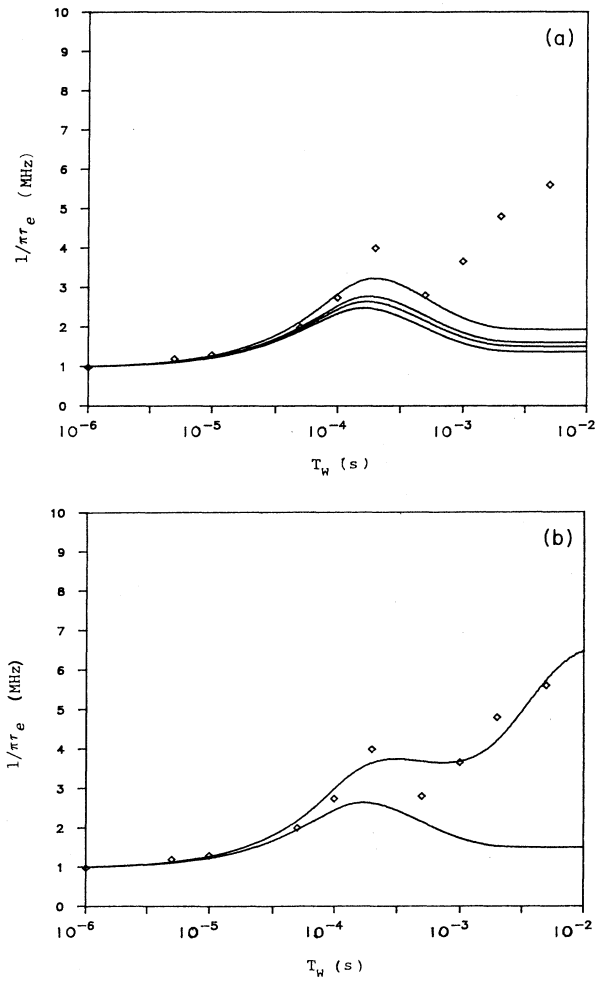

FIG. 3. Fit of Eq. (4.13) to the delayed FID experimental data (Ref. 9) from Pr^{3+}:CaF_2 crystals. The vertical axis is $1/\pi\tau_e$, where τ_e is the $1/e$ point of the FID signal. The fluctuation rate distributions are modeled as two δ functions (see text), and the rates are varied to fit the data. (a) Preliminary calculation. The rates are set at $R_0 = 5.0$ ms^{-1} and $R_1 = 0.0$ ms^{-1}; the boundary of the cutoff for the "intermediate-distance" spins is varied in the four calculated curves. From top to bottom: (1) fourth-nearest neighbors; (2) fifth-nearest neighbors; (3) sixth-nearest neighbors; (4) seventh-nearest neighbors. (b) Fit of the data using the full calculation. Upper curve: $R_0 = 5.0$ ms^{-1} and $R_1 = 0.35$ ms^{-1}, and the cutoff is the sixth-nearest neighbor. Lower curve: replot of curve 3 in (a) as a comparison. All other parameters used in the calculation are experimentally measured values. The agreement between theory and the data is very good, and the fit provides the fluctuation rates R_0 and R_1.

Setting $R_1 = 0$ we fit the early part of the curve ($T_W < 0.1$ ms) and the center of the bump by varying the value of R_0, and, for the ground-state Pr^{3+} ions, the boundary of the cutoff between the intermediate distance and the "distant" spins. It is found that the center is essentially only sensitive to the value of R_0, whereas the curvature is most sensitive to the choice of the boundary. In Fig. 3(a) the results of some of the calculations using Eq. (4.13) and the data are shown. In these calculations, R_0 is 5.0 ms^{-1}, and the boundaries are set at the fourth-nearest neighbors for curve 1, the fifth for curve 2, the sixth for curve 3, and the seventh for curve 4. The curves become essentially invariant when the boundaries are farther than the seventh-nearest neighbors.

We choose the sixth-nearest neighbors as the boundary of the cutoff between the intermediate distance and the distant spins because it gives the overall best fit. The physical justification for this boundary is that the coupling between the Pr^{3+} ion and the distant spins is weaker than the spins' "homogeneous linewidth," $\Delta\nu_{sp}$, and hence these spins flip at the free bulk rate.[36] The linewidth, $\Delta\nu_{sp}$, of the CaF_2 crystal was reported in some early NMR studies. The HWHM is found to be $\Delta\nu_{sp} = 18.4$ kHz when a strong static magnetic field is applied along the [100] crystal axis.[37] Without the applied field, this value would be about factor of $\frac{10}{3}$ larger,[37] which implies that the linewidth under consideration is about 60 kHz. Using Eq. (4.10), one can easily find that the coupling strengths for the individual spins farther than the seventh-nearest neighbors are less than 60 kHz. Thus the choice is also consistent with previous work.

After $T_W = T_0$, the signal is mainly from the persistent hole in the ground state, and the further increase of the hole width is dominated by spins flipping at R_1. Having set $R_0 = 5.0$ ms^{-1} and the boundary to be the sixth-nearest neighbor, i.e., having set spin group 3 to include the second- through the sixth-nearest neighbors, we vary R_1 to fit the data for $T_W > 0.5$ ms. $R_1 = 0.35$ ms^{-1} gives the best overall result. The final calculated curve, which results from the fitting procedure, is shown in Fig. 3(b). (Some additional details and considerations in the fitting procedure are discussed in Appendix D.) Considering the simplifications used to describe the rate distribution function, the agreement between the data and the calculation is quite good. By dividing the spins into more subgroups, a better fit was obtained. This requires a large number of free parameters and obscures the basic physics of the problem.

V. CONCLUSIONS

We have demonstrated that waiting-time-dependent dephasing measurements can be used to reveal the fluctuation-rate distributions and, hence, the dynamics, in complex systems. Using a sudden-jump model of the fluctuations, we found a general relationship between waiting-time-dependent dephasing measurements and the fluctuation-rate distribution function of a complex system, regardless of the details of the coupling form and the

spatial distributions of the perturbers. For the most general waiting-time-dependent dephasing measurement, i.e., the stimulated echo, the relation is found to be

$$\frac{\partial \ln(I_S)}{\partial T_W} \propto \int dR\, P_1(R) \exp(-RT_W) ,$$

i.e., the derivative of the echo-decay function is directly proportional to the Laplace transform of the fluctuation-rate distribution function.

Similar relationships for other waiting-time-dependent phasing measurements, such as transient hole burning, fluorescence line narrowing, or accumulated echoes, can readily be established. We also demonstrated that for any model of the fluctuations, e.g., Gaussian fluctuations, analogous relationships can be obtained. The Gaussian fluctuation problem was solved explicitly.

We applied the formal results to the problem of the dephasing of optical centers in a glassy system. Three different fluctuation-rate distributions for the glass were considered as examples. It was shown that the differences between the linewidths measured by two-pulse–echo and persistent hole-burning experiments can be explained. It was demonstrated that the shapes of the three distributions can indeed be distinguished by conducting waiting-time-dependent optical dephasing measurements. Furthermore, by conducting such experiments as a function of temperature, information on the energy-level distribution and tunneling-parameter distribution associated with the glass's two-level systems can be revealed.

The method was also applied to the analysis of optical dephasing measurements in a complex crystal. With a simple model of a two-δ-function rate distribution, the calculations successfully interpreted the time-dependent behavior of the spectral diffusion observed in the system. The agreement between the calculation and the experimental data is very good. Application of the general approach to other disordered systems, such as proteins, should be analogous.

The results provided in this paper represent a new approach to extracting dynamical information from optical line-narrowing experiments performed on complex systems. The theory also provides a unifying description of optical line-narrowing experiments and shows how experiments that operate on different time scales will provide distinct views of the same system. Finally, it is important to point out that the formalism presented here applies to magnetic resonance experiments as well as optical dephasing experiments.

ACKNOWLEDGMENTS

We would like to thank Dr. Robert Shelby for providing the details of the experiments on Pr^{3+}:CaF_2 crystals and for his stimulating discussions with us about the mechanism of optical dephasing in this system. This work was supported by the U.S. National Science Foundation Division of Materials Research (Grant No. DMR87-18959) and the U.S. Office of Naval Research (Contract No. N00014-86-K-0825).

APPENDIX A: DEPHASING INDUCED BY A SINGLE TWO-LEVEL PERTURBER: RATE-EQUATION DERIVATION

Consider the motion of a localized perturber undergoing sudden jumps between two levels. The rate equations describing the jumps can be written as

$$\begin{aligned} \frac{d\rho_{++}}{dt} &= -\rho_{++}R_{+-} + \rho_{--}R_{-+} , \\ \frac{d\rho_{--}}{dt} &= \rho_{++}R_{+-} - \rho_{--}R_{-+} , \end{aligned} \tag{A1}$$

where ρ_{++} (ρ_{--}) is the population in the upper (lower) state, and R_{-+} (R_{+-}) is the up (down) transition rate. The equations can be readily solved as

$$\begin{aligned} &\Delta\rho(t) - \Delta\rho(\mathrm{eq}) = [\Delta\rho(0) - \Delta\rho(\mathrm{eq})] \exp(-Rt) , \\ &\Delta\rho = \rho_{++} - \rho_{--}, \quad R = R_{+-} + R_{-+} , \end{aligned} \tag{A2}$$

where $\Delta\rho(\mathrm{eq})$ is the population difference at equilbrium. The equation describes the regression of the population fluctuation.

From Eq. (2.1) it is seen that the phase error induced by the perturber consists of two parts: that accumulated between $t=0$ and $t=\tau$, and that accumulated between $t=T_W+\tau$ and $t=T_W+2\tau$. In the limit of $\tau \ll T_W, 1/R$, the probability that the perturber undergoes a change of state within these two intervals is very small. The phase error φ can only be introduced in two ways: (1) $\varphi = 2\,\Delta\omega\,\tau$ if the perturber is initially in the upper state at $t=\tau$ and ends up in the lower state at $t=\tau+T_W$; (2) $\varphi = -2\,\Delta\omega\,\tau$ if the perturber is initially in the lower state at $t=\tau$ and ends up in the upper state at $t=\tau+T_W$. $2\,\Delta\omega$ is the change in the transition frequency of the optical center (the coupling strength) induced by the state change of the perturber.

A mathematically equivalent, physically more realistic, view of this dephasing process is that the optical center under consideration is initially on resonance with the laser frequency and none of the perturbers flipped during $0<t<\tau$, and there is no phase error introduced during this time period. A phase error of $2\,\Delta\omega\,\tau$ is induced in the time period $[T_W+\tau, T_W+2\tau]$ only if the perturbers flipped between τ and $T_W+\tau$, i.e., the value of the phase error is only determined by the state of the perturber at $t=T_W$. We will use this description in the future.

Using Eq. (A2), one finds the probabilities for the perturber to follow these two history paths:

$$\begin{aligned} p_{+-} &= P(\rho_{++}(0)=1) P(\rho_{--}(T_W) | \rho_{++}(0)=1) \\ &= \rho_{++}(\mathrm{eq}) \rho_{--}(\mathrm{eq}) [1 - \exp(-RT_W)] , \\ p_{-+} &= p_{+-} , \end{aligned} \tag{A3a}$$

where $P(\rho_{--}(T_W)|\rho_{++}(0)=1)$ is the conditional probability of finding the perturber in its lower state at T_W given a condition $\rho_{++}(0)=1$. The probabilities of the other two history paths can be calculated in the same manner. The results are

$$p_{++}=\rho_{++}(\text{eq})-p_{+-}\ ,$$
$$p_{--}=\rho_{--}(\text{eq})-p_{+-}\ . \tag{A3b}$$

The latter two paths do not contribute to the dephasing process. It can be verified that the sum of these probabilities is equal to unity. Thus the history average becomes

$$\begin{aligned}\langle 1-\exp(i\varphi)\rangle_H &= p_{+-}[1-\exp(2i\,\Delta\omega\,\tau)] \\ &\quad +p_{-+}[1-\exp(-2i\,\Delta\omega\,\tau)] \\ &= \operatorname{sech}^2(E/2kT)\sin^2(\Delta\omega\,\tau) \\ &\quad \times[1-\exp(-RT_W)]\ ,\end{aligned} \tag{A4}$$

which is identical to Eq. (2.5).

We should point out that the procedure used here is a more flexible approach than that used in the main text. It can be directly applied to nonexponential population relaxations. For a population relaxation of arbitrary form

$$\Delta\rho(t)-\Delta\rho(\text{eq})=[\Delta\rho(0)-\Delta\rho(\text{eq})]f(Rt)\ , \tag{A5}$$

we find the corresponding history average to be

$$\langle 1-\exp(i\varphi)\rangle_H=\operatorname{sech}^2(E/2kT)\sin^2(\Delta\omega\,\tau)[1-f(Rt)]\ . \tag{A6}$$

This formula may be used for more general cases.

APPENDIX B: GATE FUNCTION FOR THE GAUSSIAN RANDOM PROCESS

For a multilevel perturber, in the limit of $\tau\ll T_W, 1/R$ for at least some of the R in the distribution, the history average can be calculated in a manner similar to that discussed in Appendix A. Note that here R is the average rate for the perturber to change its state. In this case, the history average is a sum over all possible initial and final states of the perturber,

$$\begin{aligned}\langle 1-\exp(i\varphi)\rangle_H &= \sum_{i,j} P(\Delta\omega_j(T_W),\Delta\omega_i(0)) \\ &\quad \times\{1-\exp[i(\Delta\omega_j-\Delta\omega_i)\tau]\}\ ,\end{aligned} \tag{B1}$$

where $\Delta\omega_i$ is the coupling strength between the perturber in its ith state and the optical center, with respect to an average coupling strength, i.e., $\langle\Delta\omega\rangle=0$. The joint probability can also be written as

$$P(\Delta\omega_j(T_W),\Delta\omega_i(0))=P(\Delta\omega_i(0))P(\Delta\omega_j(T_W)|\Delta\omega_i(0))\ . \tag{B2}$$

If the total number of the levels is large (≥ 10) and the coupling strength does not vary much among the adjacent levels, $|\Delta\omega_{i+1}-\Delta\omega_i|\tau\ll 1$, the perturber can be taken to undergo a diffusive motion on an energy surface (Fokker-Planck approximation). In this case, the motion of $\Delta\omega_j(t)$ can be described approximately by a Gaussian-Markoffian process (see, for example, Ref. 38). This type of perturbation might arise from the quasicontinuous angular fluctuation of a dipole or the Brownian motion of a localized defect. The calculation of the history average for a Gaussian-Markoffian process is straightforward. The result is

$$\begin{aligned}&\langle 1-\exp(i\varphi)\rangle_H=1-\exp[-\sigma^2(\varphi)/2]\ , \\ &\sigma^2(\varphi)=\langle[\Delta\omega(T_W)-\Delta\omega(0)]^2\rangle\tau^2 \\ &\qquad =2\langle\Delta\omega^2\rangle[1-\exp(-RT_W)]\tau^2\ ,\end{aligned} \tag{B3}$$

where the steady-state condition

$$\langle[\Delta\omega(T_W)]^2\rangle=\langle[\Delta\omega(0)]^2\rangle=\langle\Delta\omega^2\rangle$$

and the relation

$$\langle\Delta\omega(T_W)\Delta\omega(0)\rangle=\langle\Delta\omega^2\rangle\exp(-RT_W)$$

have been used.

By definition, the gate function is simply proportional to the derivative of Eq. (B3),

$$\begin{aligned}&\frac{\partial\langle 1-\exp(i\varphi)\rangle_H}{\partial\ln T_W} \\ &\quad\propto RT_W\exp(-RT_W) \\ &\qquad\times\exp\{-\langle\Delta\omega^2\rangle\tau^2[1-\exp(-RT_W)]\}\ .\end{aligned} \tag{B4}$$

In this equation, however, R is coupled with $\Delta\omega$.

To derive a gate function that only varies with R and T_W, we need first to carry out the spatial average by assuming a specific spatial distribution of the perturbers and a specific coupling form $\Delta\omega(r)$. For a uniform spatial distribution and a coupling $\Delta\omega=\eta/r^n$, we have

$$\begin{aligned}&\left\langle\frac{\partial\langle 1-\exp(i\varphi)\rangle_H}{\partial\ln T_W}\right\rangle_r \\ &\quad\propto A\langle(\langle\eta^2\rangle\tau^2)^{3/2n}\rangle_{\theta,\varphi} \\ &\qquad\times[1-\exp(-RT_W)]^{3/2n-1}RT_W\exp(-RT_W)\ , \\ &A=\frac{4\pi}{n}\int dx\,x^{1-3/n}\exp(-x^2)\ ,\end{aligned} \tag{B5}$$

where $x^2=\langle\Delta\omega^2\rangle\tau^2[1-\exp(-RT_W)]$. Following the discussion in Sec. III, we find that the gate function is

$$W(u)=\exp(u-e^u)[1-\exp(-e^u)]^{3/2n-1}\ . \tag{B6a}$$

For the particular case of dipole-dipole coupling, $n=3$. We have

$$W(u)=\exp(u-e^u)/[1-\exp(-e^u)]^{1/2}\ . \tag{B6b}$$

We reason that the general form of the gate function is a function with a single peak about $u\simeq v$, with a $\Delta u\sim v=\ln(1/T_W)$. The argument is as follows.

For an arbitrary perturber, in the limit of $\tau\ll T_W, 1/R$, the history average is given by Eq. (B1). If $RT_W\gg 1$, $\Delta\omega(T_W)$ and $\Delta\omega(0)$ become completely uncorrelated, i.e.,

$$P(\Delta\omega_j(T_W),\Delta\omega_i(0))=P(\Delta\omega_j)P(\Delta\omega_i),\quad RT_W\gg 1\ .$$

As a result,

$$\langle 1-\exp(i\varphi)\rangle_H = 1-\left[\sum_j P(\Delta\omega_j)\exp(i\,\Delta\omega_j\tau)\right]^2$$

is independent of R. On the other hand, if $RT_W \ll 1$, $\Delta\omega(T_W)$ remains in its initial value, $\Delta\omega(T_W)\simeq\Delta\omega(0)$, and the probability becomes

$$P(\Delta\omega_j(T_W),\Delta\omega_i(0)) = P(\Delta\omega_j)\delta_{ji},\quad RT_W \ll 1\ .$$

which yields $\langle 1-\exp(i\varphi)\rangle_H = 0$. Clearly, the transition between these two constant values occurs at $R\simeq 1/T_W$. The behavior of $\langle 1-\exp(i\varphi)\rangle_H$ in the transition region is determined by the correlation functions (all orders) of $\Delta\omega(T_W)$. Thus we conclude that the gate function $W(u-v)$, which is proportional to the derivative of the history average, is a function with a single peak about $u\simeq v$, with a width $\Delta u\sim v = \ln(1/T_W)$.

Note that in the above discussion we assumed that R is the same for all the levels of a perturber. The distribution in R is from an ensemble of perturbers. In reality, R differs for different levels even in a single perturber. The distribution in R actually incorporates this difference.

APPENDIX C: FOUR-POINT CORRELATION FUNCTION FOR THE Pr^{3+}:CaF_2 CRYSTAL

In general, the dynamics of the perturbers can be influenced by the optical center. As a result, both the coupling strength $\Delta\omega$ and the flip rate R of a perturber are correlated to the state of the optical center. A typical example is the Pr^{3+}:CaF_2 crystal discussed in the text.

In this case, the dephasing of a single Pr^{3+} ion is dependent on its state during the waiting time T_W. If the Pr^{3+} ion is in the ground state during the entire waiting time, the surrounding spins will stay aligned with the magnetic field **B** produced by its magnetic moment. The dephasing is described by Eq. (A4). $\Delta\omega$ can be calculated with Eq. (4.10), and R is the flip rate of the individual spin under consideration.

If the Pr^{3+} ion stays in the excited state after the preparation laser pulse, its strong magnetic moment no longer exists. The surrounding spins will start to evolve to come into alignment with the new local field. Because the field is weak, the precession frequencies of the spins are slower than (or comparable to) the flip rate R_0. Note that R_0 is the free bulk flip rate that applies to all the spins. The evolution can be described as sudden jumps; each "kick" sends a spin from its old orientation to a new quantized direction. Assuming $E \ll kT$, we can write the rate equations as

$$\begin{aligned}
\frac{d\rho_{++}}{dt} &= -\rho_{++}R_0\ ,\\
\frac{d\rho_{--}}{dt} &= -\rho_{--}R_0\ ,\\
\frac{d\rho_{22}}{dt} &= (-\rho_{22}+\rho_{11})R_0/2+(\rho_{++}\sin^2\alpha+\rho_{--}\cos^2\alpha)R_0\ ,\\
\frac{d\rho_{11}}{dt} &= (\rho_{22}-\rho_{11})R_0/2+(\rho_{++}\cos^2\alpha+\rho_{--}\sin^2\alpha)R_0\ ,
\end{aligned} \tag{C1}$$

where 2α is the angle between $\mathbf{B}(t<0)$ and $\mathbf{B}(t>0)$, and ρ_{22} (ρ_{11}) is the population of the upper (lower) level along the new axis. The general solution of Eq. (C1) is

$$\begin{aligned}
\rho_{++}(t) &= \rho_{++}(0)\exp(-R_0t)\ ,\\
\rho_{--}(t) &= \rho_{--}(0)\exp(-R_0t)\ ,\\
[\rho_{22}(t)+\rho_{11}(t)] &= [\rho_{22}(0)+\rho_{11}(0)]\\
&\quad +[\rho_{++}(0)+\rho_{--}(0)]\\
&\quad \times[1-\exp(-R_0t)]\ ,\\
[\rho_{22}(t)-\rho_{11}(t)] &= [\rho_{22}(0)-\rho_{11}(0)]\exp(-R_0t)\\
&\quad +[\rho_{++}(0)-\rho_{--}(0)]\\
&\quad \times\cos(2\alpha)R_0\exp(-R_0t)\ .
\end{aligned} \tag{C2}$$

We can readily obtain the specific solution by setting $\rho_{++}(0)+\rho_{--}(0)=1$ and $\rho_{22}(0)=\rho_{11}(t)=0$.

If, at $t=T_W$, the ion is still in the excited state, we can set $t=T_W$ and calculate the history average using the same procedure as that in Appendix A. When the spin flips to align with the new axis, however, the phase errors are given by $\pm(1\pm\cos2\alpha)\Delta\omega\tau$, instead of $\pm2\Delta\omega\tau$. After an average over the random orientation, 2α, we find

$$\begin{aligned}
\langle 1-\exp(i\varphi)\rangle_H &= [1-\sin(2\,\Delta\omega\tau)/2\,\Delta\omega\tau][1-\exp(-R_0T_W)]/2\\
&\quad +\{\sin(2\,\Delta\omega\tau)/2\,\Delta\omega\tau-[\sin(\Delta\omega\tau)/\Delta\omega\tau]^2\}R_0T_W\exp(-R_0T_W)/2\ .
\end{aligned} \tag{C3}$$

If the waiting time is comparable to or longer than the excited state time $T_W \geq T_0$, most of the initially excited Pr^{3+} ions will have relaxed to the ground state. Upon relaxing to the ground state, the strong magnetic moment of the Pr^{3+} ion instantly projects the randomized spins onto the old quantization axis, since the precession frequencies are now much greater than the flip rates. Assuming the ion dropped to the ground state at $t=T_0<T_W$, and noting the relation

$$\begin{aligned}
&\Delta\rho(T_W)-\Delta\rho(\mathrm{eq})\\
&\quad =[\Delta\rho(T_0)-\Delta\rho(\mathrm{eq})]\exp[-R(T_W-T_0)]\\
&\quad =[\Delta\rho(0)-\Delta\rho(\mathrm{eq})]\exp[-R_0T_0-R(T_W-T_0)]\ ,
\end{aligned} \tag{C4}$$

we calculate the probabilities of the different history paths of the perturber to be

$$p_{+-}=p_{-+}=\rho_{++}(\mathrm{eq})\rho_{--}(\mathrm{eq}) \times\{1-\exp[-R_0T_0-R(T_W-T_0)]\}\ , \tag{C5}$$

where R_0 and R denote the fluctuation rates of the perturber at $t<T_0$ and $t>T_0$, respectively.

The phase error, which is determined by the final state of the perturber, is the same as that in Eq. (A4). Thus the resultant history average is

$$\langle 1-\exp(i\varphi)\rangle_H=\sin^2(\Delta\omega\tau) \times\{1-\exp[-R_0T_0-R(T_W-T_0)]\}\ . \tag{C6}$$

These results are used to evaluate the total dephasing of the Pr^{3+} ions in Sec. IV D.

APPENDIX D: ADDITIONAL REMARKS ABOUT THE Pr^{3+}:CaF_2 CRYSTAL DATA

This appendix contains some additional remarks about the procedure used to fit the Pr^{3+} data discussed in Sec. IV D.

Because of partial covalent bonding, which results in electronic wave-function mixing between the Pr^{3+} ion and the neighboring F^- ions, the Pr^{3+} interaction with the interstitial and the nearest-neighbor F^- ions is stronger than given by Eq. (4.10). Optically detected NMR measurements[35] show that the frequency deturning induced by the interstitial and the nearest neighbors are 20.65 and $\sim$9.5 MHz, respectively. In contrast, Eq. (4.10) would predict these values to be 6.76 and 7.37 MHz.[35] The same measurement shows that the detunings of the next-nearest neighbors (and hence the more distant spins) are essentially given by Eq. (4.10).

The measured values of the nearest spin-coupling strengths are used in the fit. Because of the finite bandwidth of the probe pulse ($\sim$6 MHz), flips of these spins only affect the size, but not the shape, of the correlation function $C_{EG}(\tau,T_W,\tau;t)$. In the case of $C_G(\tau,T_W,\tau)$, the nearest spins do not contribute because their flip rates are virtually zero. However, they do contribute to $C_E(\tau,T_W,\tau)$, because here their orientations are random. We include the contribution of the flips of these nearest spins to the correlation function $C_{EG}(\tau,T_W,\tau;t)$ by counting out the odd number flips of the eight nearest spins. This determines the depth of the persistent hole. using a binomial distribution, we find

$$C_{EG}(\tau,T_W,\tau;t)=B(t)[C_{EG}(\tau,T_W,\tau;t)]_{\text{other spins}}\ , \qquad B(t)=\sum_{k=\text{even}}^{N=8}\frac{N!}{k!(N-k)!}p^k(1-p)^{N-k}\ , \tag{D1}$$

where $p=[1-\exp(-R_0t)]/2$ is the probability of finding an individual spin flipped at t [see Appendix A, Eq. (A3a)].

The contribution of the interstitial spin is excluded. If included, the calculated burning efficiency of the persistent hole would be much too high when compared with the experimentally observed value. The environment of the interstitial spin differs from the rest of the spins. Therefore, the interstitial spin does not flip at the bulk rate when the atom is excited and does not contribute to the permanent hole.

In the treatment, the spin flips are taken to be independent events and possible correlations between the spin pairs is excluded. This is in agreement with the finding by Devoe *et al.* in a Monte Carlo study of the free-induction decay in a Pr^{3+}:LaF_3 crystal.[34] Generally, the coupling strengths of two spins to the Pr^{3+} ion are significantly different from each other. In effect, a mutual flip is quite similar to two independent flips.

[1]D. E. McCumber and M. D. Sturge, J. Appl. Phys. **34**, 1682 (1963).

[2]J. L. Skinner and D. Hsu, Adv. Chem. Phys. **65**, 1 (1986).

[3]N. A. Kurnit, I. D. Abella, and S. R. Hartmann, Phys. Rev. Lett. **13**, 567 (1964).

[4]M. J. Weber, in *Laser Spectroscopy of Solids,* edited by W. M. Yen and P. M. Selzer (Springer, New York, 1981).

[5]W. H. Hesselink and D. A. Wiersma, Phys. Rev. Lett. **43**, 1991 (1979); J. Chem. Phys. **75**, 4192 (1981).

[6]Shuji Asaka, Hiroki Nakatsuka, Masahiro Fujiwara, and Masahiro Matsoka, Phys. Rev. A **29**, 2286 (1984); Norio Morita and Tatsuo Yajima, *ibid.* **30**, 2525 (1984); R. Beach and S. R. Hartmann, Phys. Rev. Lett. **53**, 663 (1984).

[7]See, for example, M. D. Levenson, *Introduction to Nonlinear Laser Spectroscopy* (Academic, New York, 1982).

[8]B. M. Kharlamov, R. I. Personov, and L. A. Bykovskaya, Opt. Commun. **12**, 191 (1974); A. Szabo, Phys. Rev. B **11**, 4512 (1975).

[9]R. M. Macfarlane and R. M. Shelby, in *Laser Spectroscopy VI,* edited by H. P. Weber and W. Lüthy (Springer, Berlin, 1983), p. 113; R. M. Shelby and R. M. Macfarlane, J. Lumin. **31&32**, 839 (1984).

[10]C. A. Walsh, M. Berg, L. R. Narasimhan, and M. D. Fayer, J. Chem. Phys. **86**, 77 (1987).

[11]M. Berg, C. A. Walsh, L. R. Narasimhan, K. A. Littau, and M. D. Fayer, J. Chem. Phys. **88**, 1564 (1988).

[12]Y. S. Bai and M. D. Fayer, Chem. Phys. **128**, 135 (1988); Phys. Rev. B **37**, 10 440 (1988).

[13]N. Bloembergen, R. V. Pound, and E. M. Purcell, Phys. Rev. **73**, 679 (1948).

[14]E. L. Hahn, Phys. Rev. **80**, 580 (1950).

[15]T. Muramota, S. Nakanishi, and T. Hashi, Opt. Commun. **24**, 316 (1978); K. K. Rebane, and A. A. Gorokhovskii, J. Lumin. **36**, 237 (1987).

[16]W. B. Mims, Phys. Rev. **168**, 378 (1968).

[17]P. W. Anderson, B. I. Halperin, and C. M. Varma, Philos. Mag. **25**, 1 (1972); W. A. Phillips, J. Low Temp. Phys. **7**, 351 (1972); W. A. Phillips, Rep. Prog. Phys. **50**, 1657 (1987).

[18]P. Hu and S. R. Hartmann, Phys. Rev. B **9**, 1 (1974).

[19]P. Hu and L. R. Walker, Phys. Rev. B **18**, 1300 (1978).

[20]S. Mukamel and R. F. Loring, J. Opt. Soc. Am. B **3**, 595 (1986); S. Mukamel, Phys. Rev. A **28**, 3480 (1983).

[21]J. R. Klauder and P. W. Anderson, Phys. Rev. **125**, 912 (1962).
[22]See, for example, M. B. Weissman, Rev. Mod. Phys. **60**, 537 (1988).
[23]M. J. Weber, J. Lumin. **36** (1987).
[24]*Amorphous Solids: Low-Temperature Properties,* edited by W. A. Phillips (Springer, New York, 1981).
[25]R. J. Gulotty, C. A. Walsh, F. G. Patterson, W. L. Wilson, and M. D. Fayer, Chem. Phys. Lett. **125**, 507 (1986).
[26]L. R. Narasimhan, D. W. Pack, and M. D. Fayer, Chem. Phys. Lett. **152**, 287 (1988).
[27]D. L. Huber, M. M. Broer, and B. Golding, Phys. Rev. Lett. **52**, 2281 (1984); S. Hunklinger and M. Schmidt, Z. Phys. B **54**, 93 (1984).
[28]J. L. Black and B. I. Halperin, Phys. Rev. B **16**, 2879 (1977); J. L. Black, *ibid.* **17**, 2740 (1978).
[29]R. Maynard, R. Rammal, and R. Suchail, J. Phys. (Paris) Lett. **41**, L291 (1980).
[30]J. Hegarty, M. M. Broer, B. Golding, J. R. Simpson, and J. B. MacChesney, Phys. Rev. Lett. **51**, 2033 (1983).
[31]R. O. Pohl, in *Amorphous Solids: Low-Temperature Properties,* edited by W. A. Phillips (Springer, New York, 1981).
[32]M. O. Birge and S. R. Nagel, Phys. Rev. Lett. **54**, 2674 (1985).
[33]M. T. Loponen, R. C. Dynes, V. Narayanamurti, and J. P. Garno, Phys. Rev. B **25**, 1161 (1982); M. Meissner and K. Spitzmann, Phys. Rev. Lett. **46**, 265 (1981); J. Zimmermann and G. Weber, *ibid.* **46**, 661 (1981).
[34]R. G. Devoe, A. Wokaun, S. C. Raud, and R. G. Brewer, Phys. Rev. B **23**, 3125 (1981).
[35]D. P. Burum, R. M. Shelby, and R. M. Macfarlane, Phys. Rev. B **25**, 3009 (1982).
[36]N. Bloembergen, S. Shapiro, P. S. Pershan, and J. O. Artman, Phys. Rev. **114**, 445 (1959).
[37]A. Abragam, *The Principles of Nuclear Magnetism* (Oxford University Press, 1961), Chap. IV.
[38]M. C. Wang and G. E. Uhlenbeck, Rev. Mod. Phys. **17**, 323 (1945).